

Solitons supported by localized nonlinearities in periodic media

Nir Dror and Boris A. Malomed

*Department of Physical Electronics, School of Electrical Engineering,
Faculty of Engineering, Tel Aviv University, Tel Aviv 69978, Israel*

Nonlinear periodic systems, such as photonic crystals and Bose-Einstein condensates (BECs) loaded into optical lattices, are often described by the nonlinear Schrödinger/Gross-Pitaevskii equation with a sinusoidal potential. Here, we consider a model based on such a periodic potential, with the nonlinearity (attractive or repulsive) concentrated either at a single point or at a symmetric set of two points, which are represented, respectively, by a single δ -function or a combination of two δ -functions. With the attractive or repulsive sign of the nonlinearity, this model gives rise to ordinary solitons or gap solitons (GSs), which reside, respectively, in the semi-infinite or finite gaps of the system's linear spectrum, being pinned to the δ -functions. Physical realizations of these systems are possible in optics and BEC, using diverse variants of the nonlinearity management. First, we demonstrate that the single δ -function multiplying the nonlinear term supports families of *stable* regular solitons in the self-attractive case, while a family of solitons supported by the attractive δ -function in the absence of the periodic potential is completely unstable. In addition, we show that the δ -function can support *stable* GSs in the first finite bandgap in both the self-attractive and repulsive models. The stability analysis for the GSs in the second finite bandgap is reported too, for both signs of the nonlinearity. Alongside the numerical analysis, analytical approximations are developed for the solitons in the semi-infinite and first two finite gaps, with the single δ -function positioned at a minimum or maximum of the periodic potential. In the model with the symmetric set of two δ -functions, we study the effect of the *spontaneous symmetry breaking* of the pinned solitons. Two configurations are considered, with the δ -functions set symmetrically with respect to the minimum or maximum of the underlying potential.

PACS numbers: 42.65.Tg; 03.75.Lm; 05.45.Yv; 47.20.Ky

I. INTRODUCTION

In the course of the last decade, a great deal of interest has been drawn to theoretical and experimental studies of the nonlinear dynamics in systems with periodic potentials. Physical realizations of this topic are well known in nonlinear optics [1, 2] and Bose-Einstein condensates (BECs). In optical media, the periodic (lattice) potentials may be created as permanent or virtual ones (in the latter case, these are photonic lattices induced in photorefractive crystals [2, 3]). In BECs, similar potentials can be induced in the form of optical lattices (OLs), i.e., interference patterns formed by laser beams shone through the condensate. The OLs make it possible to study a great variety of dynamical effects in BECs [4, 5]. Similar periodic potentials may also be imposed by magnetic lattices [6].

It is commonly known that, in the free space, stable one-dimensional (1D) solitons exist in optical waveguides and BECs with the attractive cubic nonlinearity, while in the 2D and 3D geometry the solitons are unstable to the collapse [7]. On the other hand, it has been predicted that 2D [9–12] and 3D [9, 12] solitons can be stabilized by dint of the corresponding OLs. Moreover, low-dimensional OLs, i.e., quasi-1D and quasi-2D lattices in the 2D [12] and 3D [12, 13] space, respectively, also provide for the stabilization of fully localized multidimensional solitons. A related prediction is the existence of stable 2D [14, 15] and 3D [16] solitons in models with radial OLs.

In BECs with repulsive interactions between atoms, i.e., the repulsive intrinsic nonlinearity, solitons cannot exist in free space, but gap solitons (GSs) may be supported by the OL. The principle behind the formation of the GS is that the periodic potential can invert the sign of the effective mass of collective excitations, which may then balance the repulsive nonlinearity. In the 1D case, several species of GSs are known, which include fundamental solitons and their two- and three-peak bound complexes, in the first and second bandgaps [17, 18], and *subfundamental* solitons in the second gap (the latter means a twisted soliton squeezed into a single cell of the potential lattice, whose norm is smaller than the norm of the fundamental soliton existing at the same value of the chemical potential) [19–21]. The origin of the GS families may be traced back to bifurcations generating them from Bloch waves at edges of the bandgaps [18, 22].

Multidimensional GSs are represented by fundamental solitons [23–26] and gap-type vortices [24, 25, 29–31]. In particular, the simplest gap vortices are composed of four density peaks, and fall into two different categories: densely packed squares (alias off-site-centered vortices), in which the center is positioned around a local maximum of the OL potential [24, 29, 31], and rhombic (on-site-centered) configurations, featuring a nearly empty lattice cell in the middle [23–26]. While GS families in 2D are also generated by bifurcations from the respective Bloch waves [22, 27], there are gap-vortex families which do not originate from such bifurcations [28].

In the experiment, an effectively one-dimensional GS, composed of few hundred atoms, was created in the condensate of ^{87}Rb [32]. In another experiment, which involved a stronger OL, broad confined states were created [33]. They were interpreted as modes intermediate between the GSs and extended nonlinear Bloch waves [34].

In a different framework, solitons can be supported by a spatial modulation of the local nonlinearity (a particular case of the “nonlinearity management” [35]). In terms of solid-state physics, an effective potential structure induced by means of this method is called a *pseudopotential* [36]. Realizations of such structures are possible in optics and BECs, where they are expected to give rise to many new effects, see recent review [37]. In optical media, nonlinearity-modulation profiles can be induced by means of nonuniform distributions of resonant dopants, similar to those in resonantly-absorbing Bragg reflectors, see original works [38] and review [39]. Such dopant-density patterns can be created by means of available technology [40]. For matter waves in BECs, similar nonlinear profiles can be created via the spatial modulation of $a_s(x)$, the local value of the s -wave scattering length. Such modulations can be induced by means of the Feshbach resonance, controlled by a nonuniform dc magnetic field [41] or resonant optical field [42, 43]. It was also predicted that the Feshbach resonance may be controlled by dc electric fields [44]. Note that the Feshbach resonance allows one to create a pseudopotential corresponding to a *sign-changing* function $a_s(x)$ (actually, this is possible in the condensate of ^7Li [45]), which implies the spatial alternation between the attractive and repulsive signs of the nonlinearity.

In the context of the BECs, many works dealt with solitons and related dynamical states in the framework of 1D pseudopotential structures [46]. Nonlinear structures based on the spatial modulation of the Kerr coefficient were also considered in optics, giving rise to similar states [47]. Solitons supported by 2D pseudopotentials were theoretically studied too, with a conclusion that it is much more difficult to stabilize them than using linear OL potentials [48]. The results accumulated in the studies of solitons in nonlinear lattices are summarized in a recent review [37].

A specific example of such nonlinear pseudopotential settings is a model where the nonlinearity is concentrated at a single point, which is represented by a δ -function. A prototypical model of this type was introduced in Ref. [49]. It may represent a planar linear waveguide with a narrow nonlinear stripe embedded into it (for the case of the second-harmonic-generating quadratic nonlinearity, spatial solitons in a similar setting were considered in Ref. [50]). In terms of the BECs, localized nonlinearity may be induced through the Feshbach resonance imposed by a focused laser beam. It should be said that a more realistic model would also include a uniform background nonlinearity, as it is difficult to create a setting where it might be completely eliminated. Nevertheless, it makes sense to consider, as

the basic one, the model in which the nonlinearity is represented solely by the localized terms, as it is reasonable to assume that the weakly nonlinear background will not lead to a drastic change of the results. Extending the studies in this direction, a model of a double-well pseudopotential, based on a symmetric set of two δ -functions, or their regularized counterparts, was introduced, with the purpose of studying the spontaneous symmetry breaking (SSB) of localized modes [51]. In particular, it is possible to find full analytical solutions for symmetric, asymmetric and antisymmetric states in the model with two ideal δ -functions. In this model, where the SSB bifurcation is of the subcritical type, the symmetric solutions are stable up to the bifurcation point. Beyond this point, the symmetric states and the emerging asymmetric states are unstable, as well as all the antisymmetric ones. Symmetry breaking in a circular nonlinear lattice, with a smooth spatial modulation of a_s , was studied, in the framework of both the Gross-Pitaevskii equation (GPE) and many-body quantum system, in Ref. [52].

A natural extension of the settings outlined above is a model integrating the linear OL potential and the nonlinearity concentrated at one or two points, represented by the respective δ -functions or their regularized versions. These systems are the subject of the present work. In particular, we demonstrate that, while cusp-shaped solitons pinned to the δ -function multiplying the attractive cubic nonlinearity turn out to be unstable, the linear periodic potential readily stabilizes them. Another issue of obvious interest is whether the strongly localized repulsive nonlinearity may support GSs in finite bandgaps of the OL-induced spectrum (we demonstrate that this is possible indeed).

The rest of the paper is organized as follows. The model is formulated in section II. For the system including the single δ -function and OL potential, analytical approximations, based on the perturbation theory, are developed for the pinned modes in the first and second finite bandgaps, as well as in the semi-infinite gap, in section III. A comparison with numerical findings is performed too. Detailed results of the numerical analysis for the existence and, most important, stability of the pinned modes in the semi-infinite, first and second gaps are reported in section IV. Both the attractive and repulsive signs of the δ -functional nonlinearity are considered, for different positions of the δ -function with respect to the underlying lattice. In section V, the analysis is reported for symmetric, antisymmetric and asymmetric modes supported by a pair of the δ -functions, positioned symmetrically with respect to a maximum or minimum of the OL potential. The paper is concluded by section VI.

II. THE MODEL

The model featuring the cubic nonlinearity represented by the δ -function was introduced in Ref. [49], in the context of tunneling of interacting particles through a junction:

$$i\psi_t + \frac{1}{2}\psi_{xx} - \sigma\delta(x)|\psi|^2\psi = 0, \quad (1)$$

where ψ is the mean-field wave function in the BEC, or the local amplitude of the guided electromagnetic field in the context of optics (in the latter case, time t is replaced by the propagation distance), with $\sigma = +1$ and -1 corresponding to the repulsive and attractive nonlinearity, respectively. Obviously, Eq. (1) amounts to the simple linear equation valid at $x < 0$ and $x > 0$, $i\psi_t + (1/2)\psi_{xx} = 0$, which is supplemented by the derivative-jump condition at $x = 0$, produced by the integration of Eq. (1) over an infinitely small vicinity of $x = 0$:

$$\psi_x(x = +0) - \psi_x(x = -0) = 2\sigma |\psi(x = 0)|^2 \psi(x = 0). \quad (2)$$

Stationary states are looked for in the ordinary form, $\psi(x, t) = e^{-i\mu t}\phi(x)$, where μ is the chemical potential in BEC ($-\mu$ is the propagation constant in optics), and real function ϕ obeys equation

$$\mu\phi + (1/2)\phi'' - \sigma\delta(x)\phi^3 = 0. \quad (3)$$

An exact soliton solution to Eq. (3) with $\sigma = -1$ is obvious:

$$\phi_0(x) = Ae^{-\sqrt{-2\mu}|x|}, \quad A^2 = \sqrt{-2\mu}. \quad (4)$$

The norm of this solution,

$$N = \int_{-\infty}^{+\infty} |\psi(x)|^2 dx, \quad (5)$$

is independent of μ , taking a constant value, $N = 1$, hence the formal application of the Vakhitov-Kolokolov (VK) criterion, $dN/d\mu < 0$ [7, 53], predicts neutral stability. In fact, numerical simulations of the evolution of pinned solitons (4) with small perturbations added to them demonstrate a strong instability (not displayed here in detail):

the soliton either decays or suffers the *collapse* (formation of a singularity), if the exact norm of the perturbed soliton is, respectively, $N < 1$ or $N > 1$. These features, including the degeneracy of the norm and the instability leading to the decay or collapse, resemble those known for the 2D *Townes solitons* [7] in the free 2D space with the cubic attractive nonlinearity, or in the 1D space with the quintic nonlinearity [8]. Moreover, it is easy to find a family of *exact* analytical solutions to Eq. (1), with $\sigma = -1$, which explicitly describe the approach to the collapse at $t \rightarrow 0^-$:

$$\psi(x, t) = \sqrt{-\frac{x_0}{t}} \exp \left\{ i \left[\frac{(|x| - ix_0)^2}{2t} \right] \right\}, \quad (6)$$

where x_0 is an arbitrary real positive constant, the solution being valid at $t < 0$. Decaying solutions, at $t > 0$, are described by the same solution (6), with $-x_0$ replaced by $x_0 > 0$, the decay taking place at $t \rightarrow +\infty$. The norm of solution (6) is exactly $N = 1$ (irrespective of the value of x_0), i.e., the same as that of stationary solution (4).

In this work we introduce a natural extension of Eq. (1), adding to it the periodic OL potential, with the objective to stabilize the solitons:

$$i\psi_t + \frac{1}{2}\psi_{xx} + \varepsilon \cos(2x)\psi - \sigma\delta(x - \xi)|\psi|^2\psi = 0. \quad (7)$$

Here, the OL potential, whose period is normalized to be π , is $V(x) = -\varepsilon \cos(2x)$. In its first period, $0 \leq x < \pi$, the minimum and maximum of the potential are located, respectively, at $x = 0$ and $x = \pi/2$ (and vice versa for $\varepsilon < 0$), while the δ -function is set at $x = \xi$, which does not necessarily coincide with the minimum or maximum of the potential.

A modification of the model, which is considered in section V, deals with the nonlinearity represented by a pair of δ -functions, placed symmetrically with respect to the minimum or maximum of the periodic potential:

$$i\psi_t + \frac{1}{2}\psi_{xx} + \varepsilon \cos(2x)\psi - \sigma [\delta(x - \xi) + \delta(x + \xi)] |\psi|^2\psi = 0 \quad (8)$$

(recall the same double-delta nonlinearity, but without the OL potential, and solely with the attractive sign of the nonlinearity, $\sigma = -1$, was introduced in Ref. [51]). In this case, the asymmetry measure of stationary modes is defined as

$$\theta = \frac{\int_0^{+\infty} |\psi(x)|^2 dx - \int_{-\infty}^0 |\psi(x)|^2 dx}{\int_{-\infty}^{+\infty} |\psi(x)|^2 dx} \equiv \frac{N_+ - N_-}{N}. \quad (9)$$

Dynamical invariants of Eqs. (7) and (8) are norm N , given by Eq. (5), and the Hamiltonian (written here for the latter equation),

$$H = \int_{-\infty}^{+\infty} \left[\frac{1}{2} |\psi_x|^2 - \varepsilon \cos(2x) |\psi(x)|^2 \right] dx + \frac{1}{2} \sum_{+,-} |\psi(x = \pm\xi)|^4. \quad (10)$$

N is proportional to the number of atoms trapped in the BEC, or the total power of the trapped beam in optics. Control parameters of the models are ε and ξ , along with N .

As said above, in models with periodic potentials solitons may exist in bandgaps of the spectrum of the linearized version of the equation – either the semi-infinite gap or finite ones, separated by Bloch bands [4, 17, 18]. For the models under consideration, the spectrum is the same as in the classical Mathieu equation (it is actually displayed by means of shaded areas in Fig. 1 below).

III. PERTURBATION ANALYSIS OF THE SINGLE-DELTA MODEL

Equation (7), as well as the corresponding linear Mathieu equation, can be treated by means of the perturbation theory if the OL strength, ε , is a small parameter. Here, we consider the case when the δ -function is placed symmetrically with respect to the periodic potential, i.e., at $\xi = 0$, the objective being to construct approximate analytical solutions for GSs (gap solitons) supported by the repulsive ($\sigma = +1$) or attractive ($\sigma = -1$) point-wise nonlinearity, in the first and second finite bandgaps, as well as for ordinary solitons in the semi-infinite gap. The respective form of the stationary equation is

$$\mu\phi + (1/2)\phi'' + [\varepsilon \cos(2x) - \sigma\delta(x)\phi^2] \phi = 0, \quad (11)$$

cf. Eq. (3).

A. The first finite bandgap

1. Solutions of the linear equation

In the case of small $|\varepsilon|$, the first finite bandgap occupies a narrow interval of values of μ around $\mu = 1/2$. Accordingly, we set

$$\mu \equiv 1/2 + \nu, \quad \text{with } |\nu| \ll 1. \quad (12)$$

Then, approximate solutions corresponding to the GS in the first finite bandgap can be sought for as

$$\phi(x) = e^{-\lambda_1|x|} [A \cos(x) + B \sin(|x|)], \quad (13)$$

where λ_1 is assumed to be a small positive coefficient (subscript 1 indicates that λ_1 pertains to the first finite bandgap).

The substitution of ansatz (13) into Eq. (11), off point $x = 0$ (which corresponds to the linear equation), and the subsequent analysis following the usual perturbation theory for the Mathieu equation (in other words, the asymptotic analysis of the linear parametric resonance [54]), yield the following equations for amplitudes A and B :

$$\begin{cases} \left[\nu + \frac{1}{2} (\lambda_1^2 + \varepsilon) \right] A - \lambda_1 B = 0, \\ \left[\nu + \frac{1}{2} (\lambda_1^2 - \varepsilon) \right] B + \lambda_1 A = 0. \end{cases} \quad (14)$$

The solvability condition for the linear homogeneous system (14) is

$$\left(\nu + \frac{1}{2} \lambda_1^2 \right)^2 - \frac{\varepsilon^2}{4} + \lambda_1^2 = 0. \quad (15)$$

In the first approximation, $\lambda_1^2/2$ may be neglected in the parentheses, which yields

$$\lambda_1 \approx \sqrt{\frac{\varepsilon^2}{4} - \nu^2}, \quad (16)$$

hence the solution exists for

$$|\nu| < |\varepsilon|/2. \quad (17)$$

In fact, Eq. (17) is the prediction provided by the perturbation theory for the width of the first finite bandgap, see Fig. 1(a). Further, it follows from Eqs. (14) that, in the first approximation,

$$B = \text{sgn}(\varepsilon) \sqrt{\frac{\varepsilon/2 + \nu}{\varepsilon/2 - \nu}} A, \quad (18)$$

where condition (17) is taken into regard, to identify the correct sign.

2. The nonlinear part of the solution

For the stationary solutions, condition (2) takes the form of

$$\Delta \left(\frac{d\phi}{dx} \right) \Big|_{x=0} = 2\sigma\phi^3 \Big|_{x=0}, \quad (19)$$

where Δ stands for the jump of the derivative at $x = 0$. The substitution of Eqs. (13), (16), and (18) into Eq. (19) yields

$$- \left(\sqrt{\frac{\varepsilon^2}{4} - \nu^2} - \text{sgn}(\varepsilon) \sqrt{\frac{\varepsilon/2 + \nu}{\varepsilon/2 - \nu}} \right) A = \sigma A^3. \quad (20)$$

On the left-hand side of Eq. (20), the term $\sqrt{\varepsilon^2/4 - \nu^2}$ is much smaller than the following term [in the general case, $\sqrt{\varepsilon^2/4 - \nu^2}$ is small, while $\sqrt{(\varepsilon/2 + \nu)/(\varepsilon/2 - \nu)}$ is not; in special cases, near the upper edge of the bandgap for $\varepsilon > 0$, or the lower one for $\varepsilon < 0$, with $|\varepsilon/2 + \nu| \ll |\varepsilon/2 - \nu|$, the term $\sqrt{(\varepsilon/2 + \nu)/(\varepsilon/2 - \nu)}$ becomes small, but $\sqrt{\varepsilon^2/4 - \nu^2}$ is then still smaller]. Thus, Eq. (20) yields, for nontrivial solutions ($A^2 \neq 0$):

$$A^2 \approx \sigma \operatorname{sgn}(\varepsilon) \sqrt{\frac{\varepsilon/2 + \nu}{\varepsilon/2 - \nu}}. \quad (21)$$

This solution exists provided that $\operatorname{sgn}(\varepsilon) = \sigma$, and it does not exist in the opposite case. In other words, it exists if the *repulsive* δ -function, with $\sigma = +1$, is set at the local *minimum* of the OL potential, or the *attractive* δ -function is placed at the local *maximum*. Note that, although the result was obtained by means of the perturbation theory, the amplitude given by Eq. (21) is not small (which does not invalidate the perturbative treatment).

In the first approximation, the calculation of the norm of the weakly localized soliton solution based on the above formulas yields

$$N_1 \approx (2\lambda_1)^{-1} (A^2 + B^2) \equiv \frac{|\varepsilon|}{2(\varepsilon/2 - \nu)^2}. \quad (22)$$

In the case of the attraction (then, ε is negative, as shown above), relation (22) yields

$$\frac{dN_1}{d\mu} \equiv \frac{dN_1}{d\nu} = -\frac{\varepsilon}{(\varepsilon/2 - \nu)^3} < 0, \quad (23)$$

hence, according to the VK criterion, the so predicted family of the GSs might be stable. Nevertheless, it is actually unstable, as shown below. As for the repulsive nonlinearity, the VK criterion is irrelevant for it (being sometimes replaced by an ‘‘anti-VK’’ condition [55]).

The calculation of Hamiltonian (10) in the present approximation yields

$$H \approx \frac{|\varepsilon|}{4(\varepsilon/2 - \nu)^2} \quad (24)$$

[in this approximation, H is dominated by the gradient term in Eq. (10)]. The fact that this expression is always positive demonstrates that the GS cannot realize a ground state (it cannot correspond to an absolute minimum of the energy, which must be either negative or zero). Nevertheless, this does not mean that these solitons cannot be stable against small perturbations (actually, they may be *metastable* states, in comparison with the ground state).

3. Comparison with numerical results

The first finite bandgap, as predicted by the perturbation theory [Eq. (17)], is shown in Fig. 1(a), together with the numerically found borders of the first bandgap. In accordance with the above prediction, the soliton in the model with the repulsive or attractive nonlinearity exists only for $\varepsilon > 0$ and $\varepsilon < 0$, respectively (this conclusion is true for all values of ε and μ in the first bandgap, not only for small ε).

As concerns the stability, the GSs supported by the repulsive δ -function placed at the minimum of the OL potential ($\sigma = +1$, $\varepsilon > 0$) are *stable*, while all the solitons generated in the finite bandgap by the attractive nonlinearity ($\sigma = -1$, $\varepsilon < 0$) are unstable [on the contrary to the formal prediction of the VK criterion, see Eq. (23)]. The detailed stability analysis is reported in the next section.

Typical profiles of the soliton solutions are shown in Figs. 2 and 3. If ε is not too large, the approximation quite accurately predicts the shape of the soliton. In particular, the analytical and numerical results agree very well for μ taken near the middle of the bandgap. Close to the upper edge (for $\varepsilon > 0$) or lower edge (for $\varepsilon < 0$), the analytical shape of the soliton is less accurate, as seen in Figs. 2(c),(f) and 3(a),(d). In fact, this inaccuracy originates from the use of approximation (21) instead of the more general equation (20).

Figure 4 shows the norm of the solitons versus μ , for both negative and positive ε , which correspond to the attractive and repulsive nonlinearities, respectively. As expected, the results become more accurate as $|\varepsilon|$ diminishes, while μ takes values farther from the upper or lower edges of the bandgap, for $\varepsilon > 0$ and $\varepsilon < 0$, respectively.

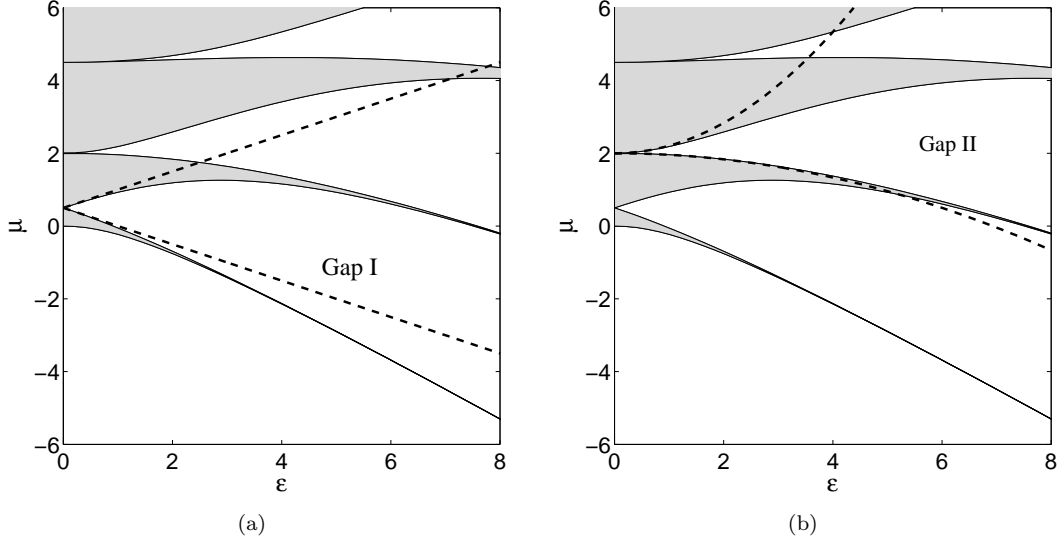


FIG. 1. Borders of the first (a) and second (b) finite bandgaps (labeled as Gap I and Gap II, respectively), as predicted by the perturbation approximation, see Eqs. (17) and (32), in comparison with the numerically constructed bandgap structure, in which Bloch bands are shaded. The semi-infinite gap is represented by the white areas at the bottom of the panels.

B. The second finite bandgap

The perturbation theory for the Mathieu equation may also uncover the second finite bandgap, when

$$\mu = 2 + \nu, \quad \text{with } |\nu| \ll 1, \quad (25)$$

cf. Eq. (12). To this end, an approximate solution to the linear equation is looked for as

$$\phi(x) = e^{-\lambda_2|x|} [A_0 + A_2 \cos(4x) + B_2 \sin(4|x|) + A_1 \cos(2x) + B_1 \sin(2|x|)], \quad (26)$$

cf. ansatz (13) adopted in the first finite bandgap. Substitution ansatz (26) into Eq. (11), off point $x = 0$, and neglecting terms $\sim \lambda_2$, we find, in the zeroth-order approximation,

$$A_0 = -\frac{\varepsilon}{4}A_1, \quad A_2 = \frac{\varepsilon}{12}A_1, \quad B_2 = \frac{\varepsilon}{12}B_1. \quad (27)$$

Next, the homogeneous system of equations for A_1 and B_1 takes the following form, cf. Eqs. (14) derived in the first finite bandgap:

$$\nu A_1 + \frac{1}{2}\lambda_2^2 A_1 + \varepsilon \left(A_0 + \frac{1}{2}A_2 \right) - 2\lambda_2 B_1 = 0, \quad (28)$$

$$\nu B_1 + \frac{1}{2}\lambda_2^2 B_1 + \frac{1}{2}\varepsilon B_2 + 2\lambda_2 A_1 = 0, \quad (29)$$

or, on substituting expressions (27),

$$\begin{aligned} \left(\nu - \frac{5\varepsilon^2}{24} + \frac{\lambda_2^2}{2} \right) A_1 - 2\lambda_2 B_1 &= 0, \\ \left(\nu + \frac{\varepsilon^2}{24} + \frac{\lambda_2^2}{2} \right) B_1 + 2\lambda_2 A_1 &= 0. \end{aligned} \quad (30)$$

Like in the case of Eqs. (14), terms $\lambda_2^2/2$ in the parentheses may be neglected in the lowest approximation, which yields

$$\lambda_2 \approx \frac{1}{2} \sqrt{\frac{5}{576}\varepsilon^4 + \frac{1}{6}\varepsilon^2\nu - \nu^2}. \quad (31)$$

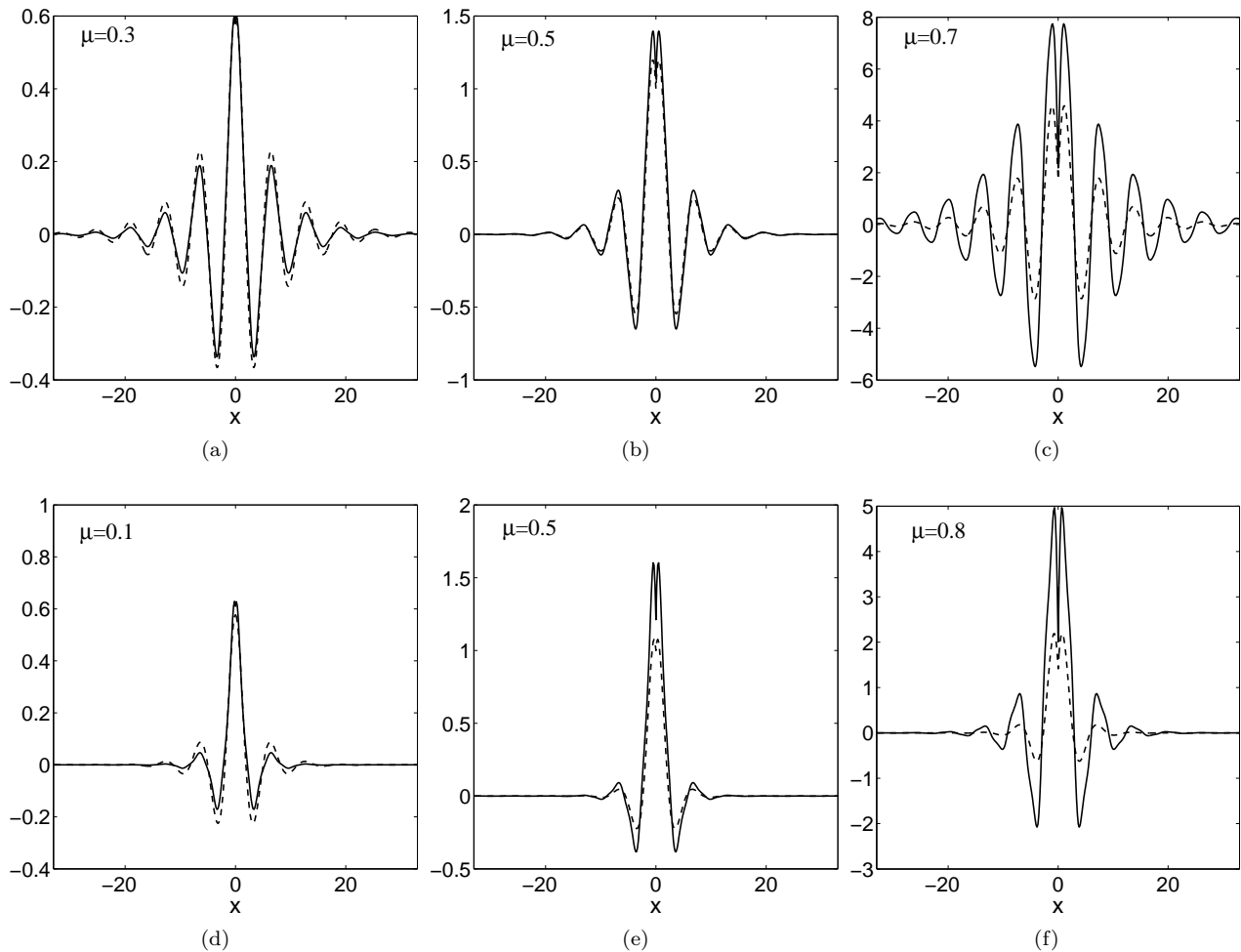


FIG. 2. Comparison between the analytical approximation (dashed lines) and the numerically found profiles (solid lines) for solitons in the first finite bandgap of the repulsive model, for $\varepsilon = 0.5$ (a)-(c) and $\varepsilon = 1$ (d)-(f). The results are shown for selected values of μ (indicated in each panel), close to the center of the gap or near each of its edges.

As follows from this expression, the perturbation theory predicts the following form of the second finite bandgap, see Fig. 1(b):

$$-1/24 \leq \tilde{\nu} \equiv \nu/\varepsilon^2 \leq 5/24, \quad (32)$$

cf. Eq. (17) for the first finite bandgap. Then, in the lowest approximation, the relation between B_1 and A_1 is [cf. Eq. (18)]

$$B_1 = -\frac{(5\varepsilon^2/24) - \nu}{2\lambda_2} A_1. \quad (33)$$

Further, the jump condition at point $x = 0$ keeps the form of Eq. (19), and, in the lowest approximation, the jump of the first derivative is dominated by term $B_1 \sin(2|x|)$ in ansatz (26). With regard to relation (33), this leads to the following prediction for the solution supported by the single δ -function in the second finite bandgap:

$$A_1^2 = -\frac{\sigma}{\lambda_2} \left(\frac{5}{24} \varepsilon^2 - \nu \right). \quad (34)$$

As follows from Eqs. (34), inside the second finite bandgap (32) this solution exists for $\sigma = -1$, i.e., solely for the *attractive nonlinearity*.

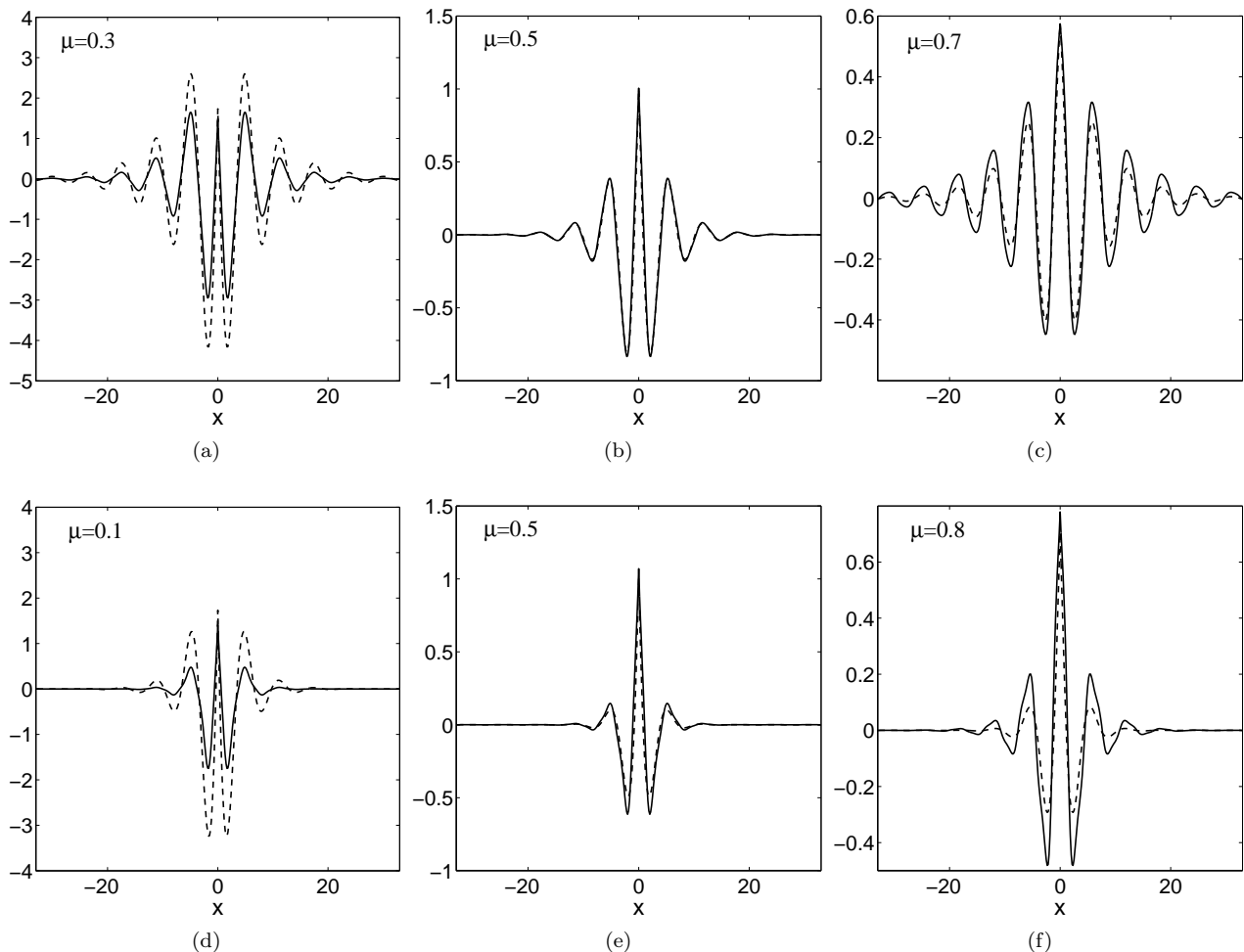


FIG. 3. The same as in Fig. 2, but for the attractive nonlinearity. In panels (a)-(c), $\varepsilon = -0.5$, and in (d)-(f), $\varepsilon = -1$.

In the first approximation, the norm of the soliton is

$$N_2 \approx \frac{2}{\varepsilon^2} \frac{(5/24) - \tilde{\nu}}{(5/576) + (\tilde{\nu}/6) - \tilde{\nu}^2} \left[1 + \frac{((5/24) - \tilde{\nu})^2}{(5/576) + (\tilde{\nu}/6) - \tilde{\nu}^2} \right], \quad (35)$$

with $\tilde{\nu}$ defined as per Eq. (32). It follows from the plot of the norm versus μ , which is shown in Fig. 5 for $\varepsilon = \pm 1$, that the corresponding GS family satisfies the VK criterion, $dN/d\mu < 0$. Nevertheless, as well as in the case of the solitons in first finite bandgap, which was considered above, the GSs in the second bandgap, supported by the attractive nonlinearity, turn out to be unstable at all values of ε .

In the general case, when the δ -function is placed asymmetrically with regard to the OL potential, GSs may exist in the second bandgap in the case of the repulsive nonlinearity, and may be *stable* in that case. A detailed analysis of this case is presented in the next section.

Examples of numerically found profiles of the solitons in the second finite bandgap, together with their analytically predicted counterparts [see Eqs. (33) and (34)], are displayed in Fig. 6. The results shown in both Figs. 6 and 5 demonstrate that the perturbative approximation is more accurate for smaller and positive values of ε , when the attractive δ -function is set at a local minimum of the OL potential.

C. The semi-infinite gap

For the sake of completeness of the analysis, we also present results of the application of the perturbation theory (for small $|\varepsilon|$) to solitons supported by the attractive δ -function ($\sigma = -1$) in the semi-infinite gap, i.e., at $\mu < 0$. In

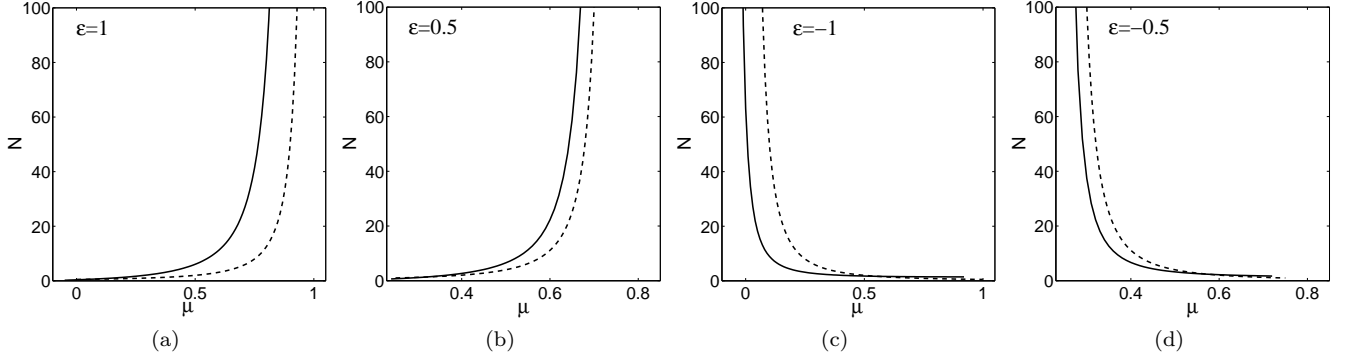


FIG. 4. The norm of the solitons in the first finite bandgap, as a function of μ . Examples for the repulsive nonlinearity are given for $\varepsilon = 1$ (a) and $\varepsilon = 0.5$ (b), and the attractive model is demonstrated for $\varepsilon = -1$ (c) and $\varepsilon = -0.5$ (d). Numerical results and the analytical approximation are depicted by solid and dashed lines, respectively.

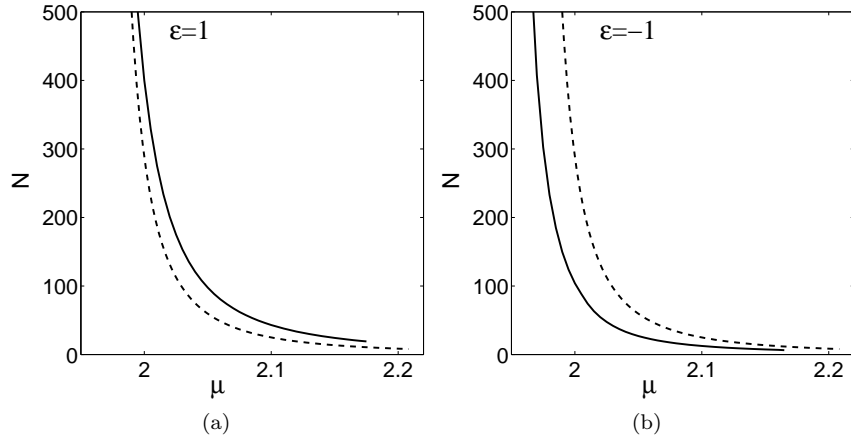


FIG. 5. The norm of the analytically predicted (dashed curves) and numerically found (solid curves) solitons in the second bandgap as a function of μ , for $\varepsilon = 1$ (a) and $\varepsilon = -1$ (b), in the case of the attractive nonlinearity.

the zeroth approximation ($\varepsilon = 0$), the soliton is given by solution (4). Then, it is easy to find the first-order correction to it in the following form:

$$\phi_1(x) = \frac{\varepsilon}{1-2\mu} \phi_0(x) \left[-\frac{5}{6} + \frac{1}{2} \cos(2x) + \sqrt{-\frac{\mu}{2}} \sin(2|x|) \right], \quad (36)$$

where $\phi_0(x)$ is expression (4) [to the first order in ε , solution $\phi_0(x) + \phi_1(x)$ satisfies both the linear part of Eq. (11) at $x \neq 0$, and the jump condition (19) at $x = 0$]. To the same order, the norm of this solution is

$$N = 1 - \frac{\varepsilon(5+2\mu)}{3(1-2\mu)^2}, \quad (37)$$

which demonstrates that the weak OL potential lifts the degeneracy of the soliton family (4). Note that expression (37) satisfies the VK stability criterion,

$$\frac{dN}{d\mu} = -\frac{2\varepsilon(11+2\mu)}{3(1-2\mu)^3} < 0, \quad (38)$$

for $\mu > -5.5$ in the case of $\varepsilon > 0$, which corresponds to the attractive δ -function set at a local minimum of the OL potential, see Eq. (11); the change of the sign of $dN/d\mu$ at $\mu < -5.5$ does not really matter, as dependence (37) is virtually flat in that region.

Numerical results demonstrate that the entire soliton family is stable in the case of $\varepsilon > 0$, obeying the VK criterion everywhere in the semi-infinite gap (for a further discussion, see the next section). Figure 7 presents the respective

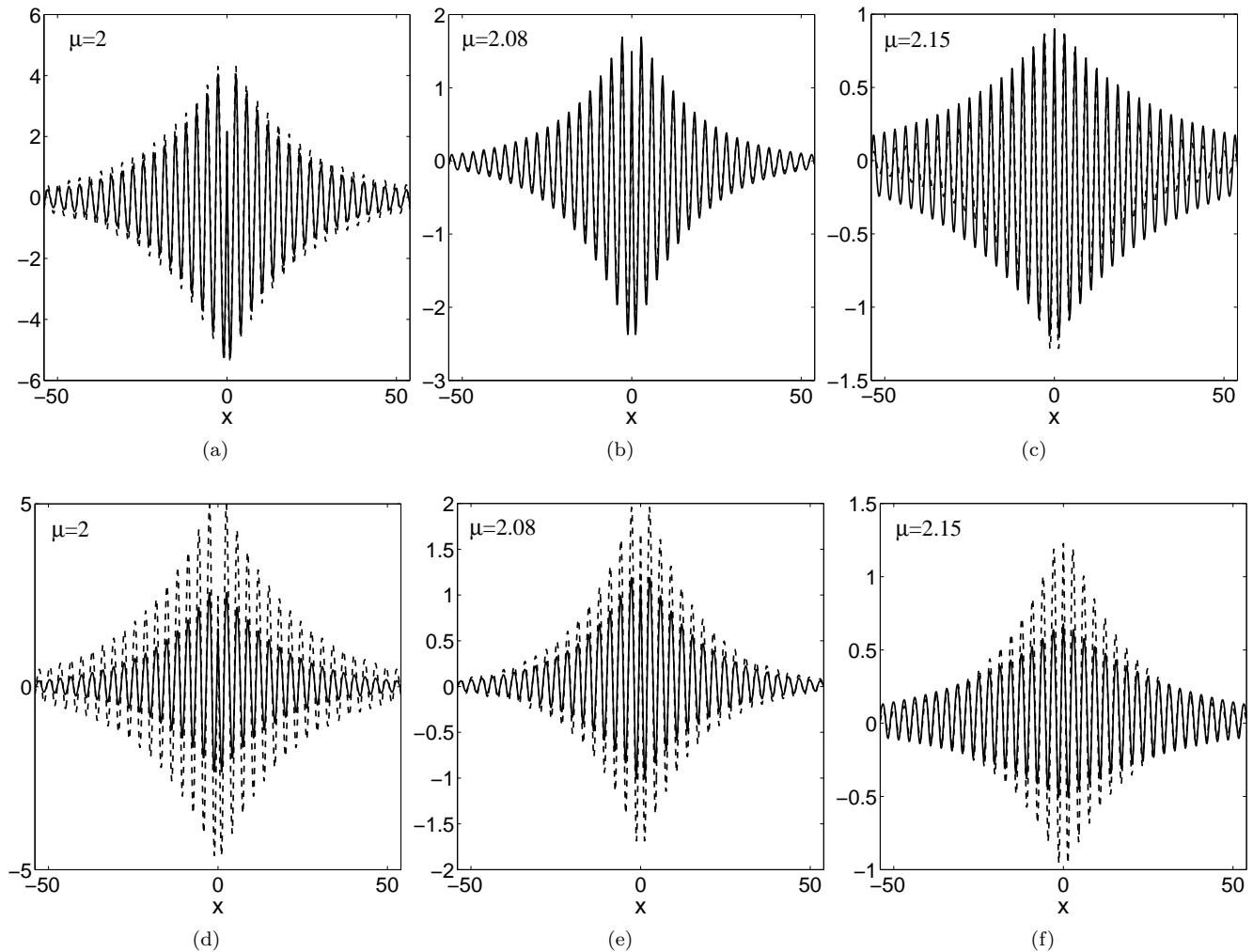


FIG. 6. Typical examples of broad profiles of the solitons in the second finite bandgap, for $\varepsilon = 1$ (a)-(c) and $\varepsilon = -1$ (d)-(f). The respective values of μ are indicated in each panel. Solid curves depict numerically found profiles, whereas the dashed lines represent the analytical prediction given by Eqs. (33)-(34).

comparison between the analytical approximation and the numerical results. As expected, the prediction is more accurate for smaller ε , closely approximating even complex soliton profiles near the edge of the gap, see panel (e) in Fig. 7. On the other hand, the solitons centered at the local maximum of the OL potential at $\varepsilon < 0$ are definitely unstable (not shown here in detail).

IV. NUMERICAL RESULTS FOR THE MODEL WITH THE SINGLE δ -FUNCTION

In the case when the local nonlinearity is represented by the single δ -function in Eq. (7), we have found soliton modes in the semi-infinite and two lowest finite gaps, and their stability was investigated by means of numerical methods. The stationary solutions were constructed applying the Newton-Raphson method to the respective nonlinear boundary-value problem. The stability was then examined by considering a perturbed solution to Eq. (7), in the form of

$$\phi(x, t) = \phi_s(x) + g e^{-i\lambda t} + f^* e^{i\lambda^* t}, \quad (39)$$

where $\phi_s(x)$ is the stationary solution, functions g and f are eigenmodes of the infinitesimal perturbation, and λ is the corresponding eigenvalue, which may be complex in the general case. When substituting expression (39) into Eq. (7)

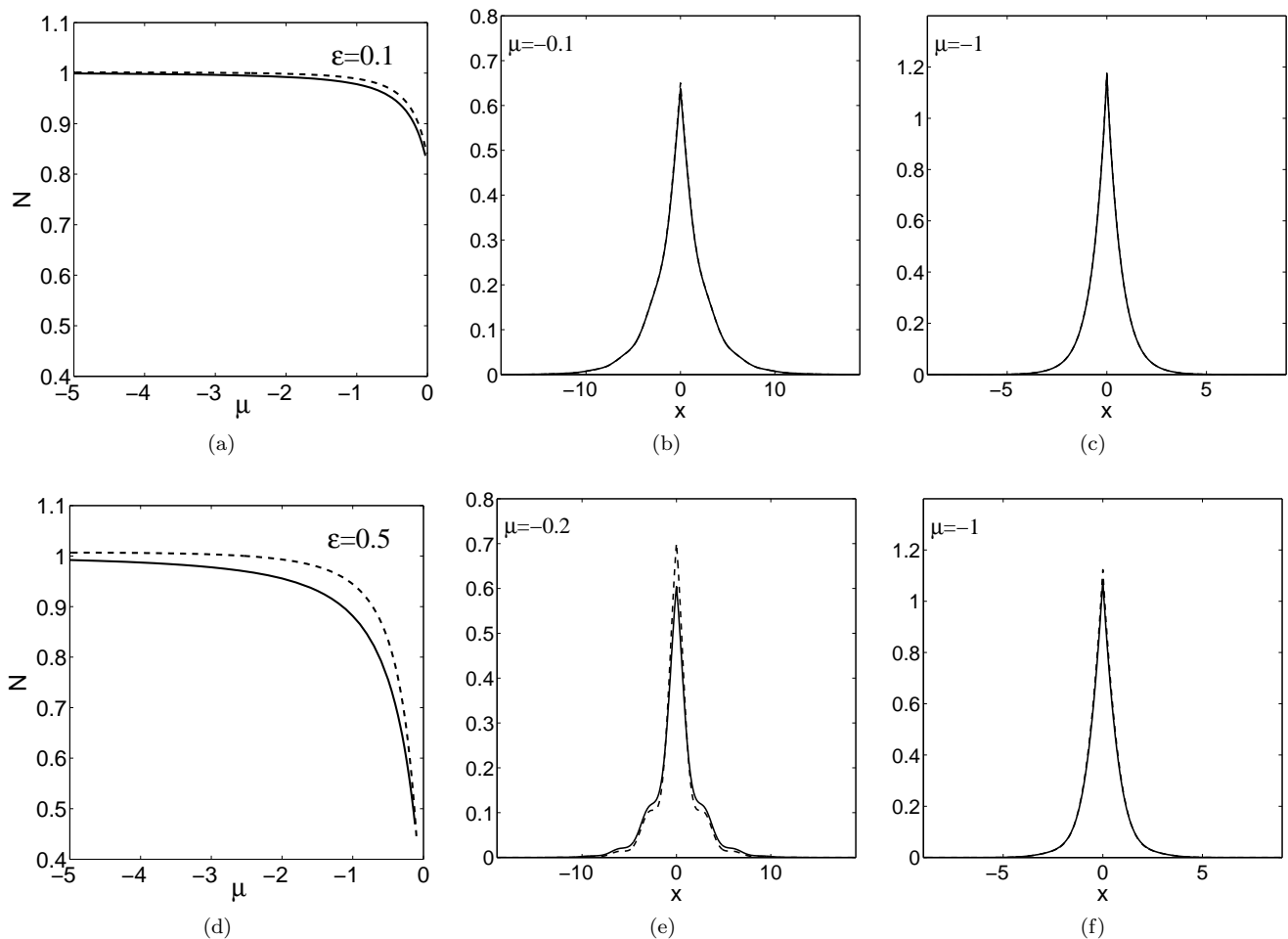


FIG. 7. Panels (a) and (d) display the comparison between the numerical and analytically estimated norms (the solid and dashed curves, respectively) for the solitons in the semi-infinite gap, for $\epsilon = 0.1$ and 0.5 , respectively. Examples of the soliton profiles, taken close to the edge of the gap and deeper inside, are displayed in panels (b),(c) and (e),(f), for the cases corresponding to (a) and (d), respectively. In (b) and (c), the analytically predicted profiles are very close to their numerical counterparts, making the dashed and solid lines virtually indistinguishable.

and linearizing, one arrives at the following eigenvalue problem:

$$\begin{pmatrix} \hat{L} & \sigma\delta(x-\xi)(\phi_s(x))^2 \\ -\sigma\delta(x-\xi)(\phi_s(x))^2 & -\hat{L} \end{pmatrix} \begin{pmatrix} g \\ f \end{pmatrix} = \lambda \begin{pmatrix} g \\ f \end{pmatrix}, \quad (40)$$

with $\hat{L} \equiv -\mu - (1/2)d^2/dx^2 - \epsilon \cos(2x) + 2\sigma\delta(x-\xi)(\phi_s(x))^2$. This problem can be easily solved using a simple finite-difference scheme, the solution being stable if all the eigenvalues are real.

The so predicted stability or instability was verified by means of direct simulations of the evolution of initially perturbed modes. For this purpose, the standard pseudospectral split-step method and the Crank-Nicolson finite-difference algorithm were used. In the course of the analysis, the δ -function was set at different positions within half a period of the OL, $0 < \xi < \pi/2$. In the numerical calculations based on the discretization with stepsize Δx , the discrete counterpart of the δ -function was defined so that it took a nonzero value, $\tilde{\delta} = 1/(2\Delta x)$, at the single point, $x = \xi$.

A. Solitons in the semi-infinite gap

Numerical analysis of the solutions in the semi-infinite gap reveals a single soliton family, which exists only in the case of the attractive nonlinearity ($\sigma = -1$). A natural result of the stability analysis is that these solitons are stable

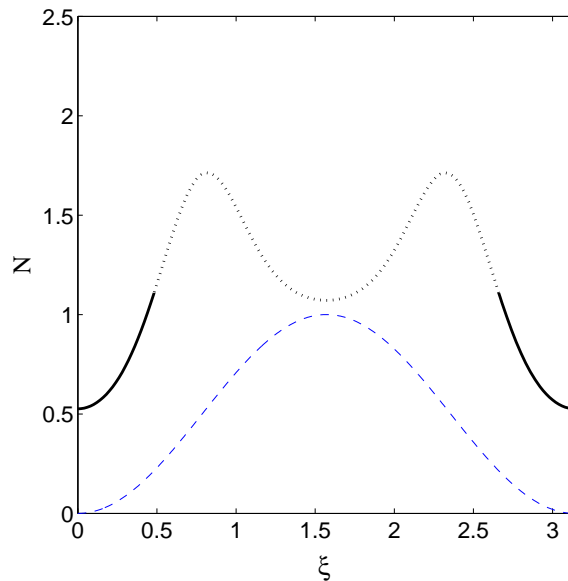


FIG. 8. (Color online) The norm versus the position of the attractive δ -function, for the soliton family in the semi-infinite gap, at $\varepsilon = 5$ and $\mu = -4$. Here and in similar figures shown below, the dashed line depicts the underlying periodic potential (rescaled and shifted upward for the clarity of the picture), while stable and unstable solitons correspond to continuous and dotted lines, respectively.

if the attractive δ -function is located at or near the minimum of the potential. An example for $\varepsilon = 5$ and $\mu = -4$ is displayed in Fig. 8, where shift ξ of the δ -function from the potential minimum, $x = 0$, takes values within a half of the spatial period of the potential (recall the period is π). In the semi-infinite gap, the soliton's stability complies with the VK criterion. In particular, the soliton family is completely stable for $\xi = 0$. On the other hand, the family is (quite naturally) completely unstable for $x = \pi/2$, when the δ -function is set at the point of the potential maximum.

B. Solitons in the first finite bandgap

The numerical analysis of solutions in the first bandgap demonstrates that GSs cannot exist *simultaneously* for the attractive and repulsive nonlinearities. If the δ -function is set close to a maximum of the potential ($\xi = \pi/2$, for $\varepsilon > 0$), it can support a soliton only with the attractive sign of the nonlinearity. Shifting the position of the attractive δ -function towards an adjacent minimum of the potential, the soliton ceases to exist at a critical (threshold) value of the coordinate, $\xi = \xi_{\text{thr}}$. At the same point, a new soliton appears in the repulsive case, and exists at $\xi < \xi_{\text{thr}}$. Figure 9(a) describes the norm of the GS versus the δ -function's position within a half of the OL period, for $\varepsilon = 5$ and $\mu = -1$, which is close to the middle of the first finite bandgap. These results agree with the prediction of the perturbation theory obtained for $x = 0$, according to which the soliton exists only for $\sigma = \text{sgn}(\varepsilon)$, see Eq. (21) (recall that $\varepsilon > 0$ and $\xi = \pi/2$ are equivalent to $\varepsilon < 0$ and $\xi = 0$). Close to the existence threshold, the amplitude of the soliton diverges, while its width remains approximately constant. Representative examples of such GSs are displayed in Fig. 10. In particular, Figs. 10(e)-(f) demonstrate a stable soliton (supported by the repulsive nonlinearity) featuring an especially high amplitude, achieved at $x = 0.282$. The threshold value, ξ_{thr} , varies with ε and μ , as shown in Fig. 11. Specifically, for small values of ε and/or small values of μ (close to the lower edge of the first bandgap), the soliton-existence region expands in the case of the repulsive nonlinearity.

The stability analysis demonstrates that, in the case corresponding to Fig. 9(a), the GSs in the first bandgap, supported by the repulsive δ -function, are *always stable*. On the other hand, in the case of the attractive nonlinearity, local unstable eigenmodes exist, with large ($\text{Im}\{\lambda\} > 1$) purely imaginary eigenvalues, making all the solitons unstable. This finding is not surprising because, as stressed above, in the cases of the repulsion and attraction the GSs tend to be located, respectively, close to a local minimum or maximum of the periodic potential.

The stability analysis was also carried out for other values of ε and μ . The solitons are always stable under the repulsive nonlinearity, while the stability may change in the case of the attraction. Examples are presented in Fig. 12(b)-(e), for $\varepsilon = 5$ and $\xi = 0.15$ (repulsion) and $\xi = 0.4, 0.7, 1.1$ (attraction). In the latter case, it is seen that, for μ close to the upper edge of the first bandgap, there are small stability areas for the solitons (conspicuous

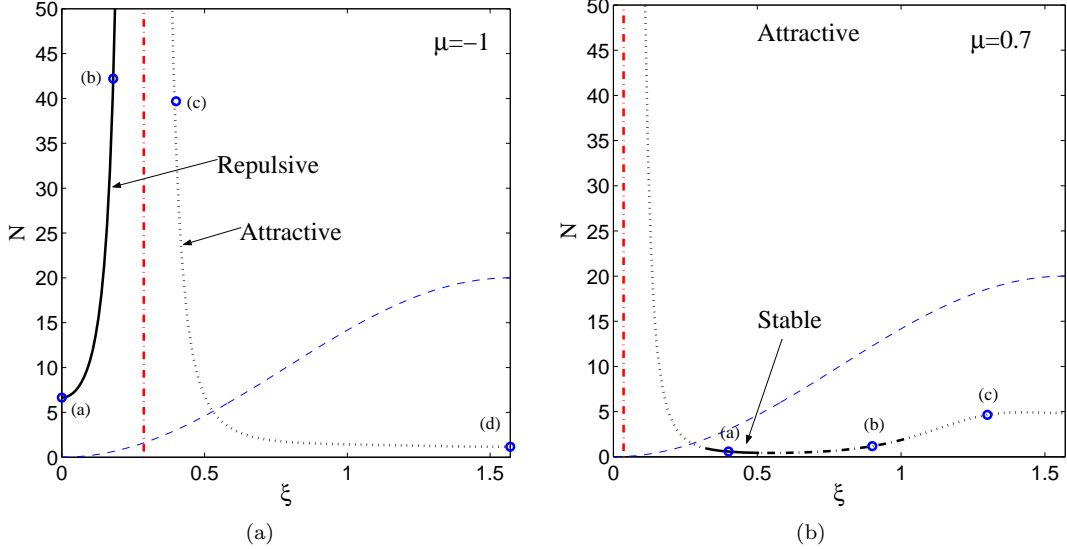


FIG. 9. (Color online) The norm versus the position of the nonlinearity-modulating δ -function, for solitons in the first finite bandgap, with $\varepsilon = 5$ and $\mu = -1$ (a) or $\mu = 0.7$ (b), and both signs of the nonlinearity. The dashed-dotted vertical lines represent the respective thresholds, $\xi_{\text{thr}} = 0.287$ (a) and $\xi_{\text{thr}} = 0.035$ (b). As before, continuous lines refer to stable solitons, while dotted and dashed-dotted ones correspond to the strong localized and weak oscillating instabilities, respectively. Shapes of the solitons corresponding to marked points in (a) are displayed in Fig. 10. The evolution of the solitons marked in (b) is displayed in Fig. 13. In panel (b), only the soliton branch corresponding to the attractive nonlinearity appears, as the region of ξ for the repulsive sign is too small, while the corresponding solitons have a very large norm.

for $\xi = 0.4$, and extremely small for larger ξ). For fixed $\mu = 0.7$ and varying position ξ of the attractive δ -function, a small stability region is found too, as shown in Fig. 9(b). Although it is small, the existence of the stability area for the GSs in the case of the attraction is a remarkable fact, as it is often assumed that all solitons are unstable in finite bandgaps, if the nonlinearity is attractive (see, however, Ref. [18], where stable GSs were found in the case of attraction). Apart from the common “localized” instability discussed above (indicated in the stability diagrams by dotted lines), there is additional weaker instability which is often referred to as “oscillatory” one (see Refs. [17, 18] for more details). This instability is characterized by complex eigenvalues, λ , and delocalized oscillatory eigenfunctions. Techniques which can be used for the detection of such instabilities are described in Ref. [18]. Regions corresponding to unstable solitons of this type can be clearly seen in Fig. 9(b), distinguished in this and other figures by a dashed-dotted marking. The oscillatory instability can also be found in the case presented in Fig. 12(e), within a tiny area between the non-oscillating unstable solitons and the region of stable solitons, which is very small by itself. Figure 13 illustrates the stability and the simulated development of the solitons’ instabilities, for the representative cases marked in Fig. 9(b).

It is relevant to stress that the stability investigation was carried out repeatedly, varying the size of the spatial domain and the number of grid points. By doing so, we have checked that the stable solitons exist indeed, not being simply a case of a weak instability.

Looking at Fig. 12, it is easy to conclude that, unlike the semi-infinite gap, the stability of the GSs in the first finite bandgap does not obey the VK criterion (cf. Ref. [55], where the same conclusion was made for models with combined linear and nonlinear periodic potentials). Another noteworthy fact is that, when the δ -function is placed anywhere except maxima or minima of the potential ($x = 0, \pi/2$), the GS family does not completely fill the first bandgap. For instance, for $\xi = 0.7$, the lower cutoff (existence border) for the soliton in the model with attraction is $\mu_{\text{thr}} \approx -2.5$, while the lower border of the bandgap is at $\mu = -2.894$.

C. Soliton solutions in the second finite bandgap

The numerical investigation was also performed for GSs in the second finite bandgap. For the repulsive nonlinearity, a single branch of solitons exists in one half of the potential period in the (N, ξ) plane. On the other hand, in the case of the attractive nonlinearity, there are *two* different branches, one located around the minimum of the potential and the other one – around its maximum. A typical example is shown in Fig. 14(a), for $\varepsilon = 5$ and $\mu = 2$, close to

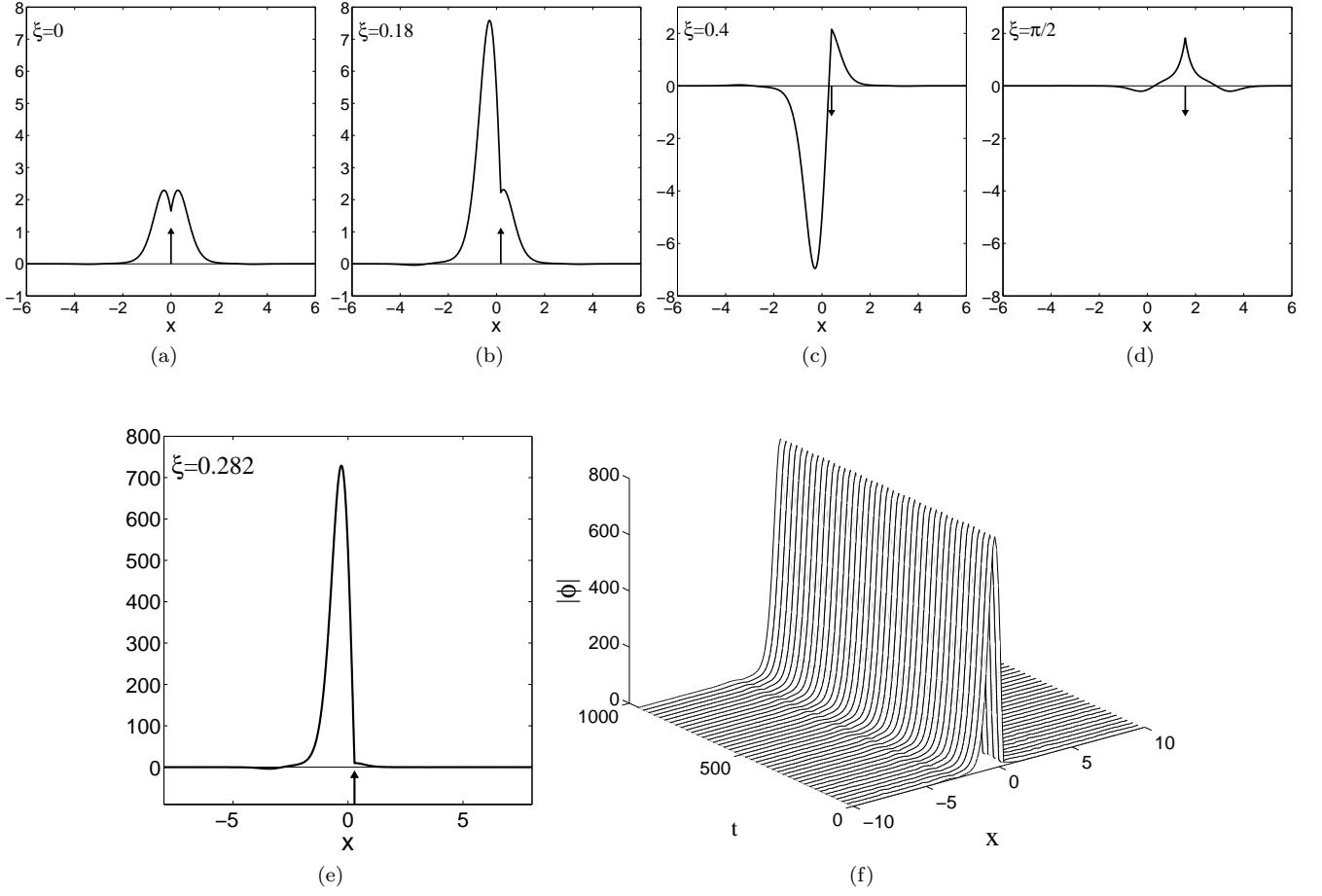


FIG. 10. Shapes of the solitons in the first finite bandgap, for the repulsive (a)-(b) and attractive (c)-(d) single- δ -function nonlinearities. The solitons correspond to marked points in Fig. 9(a), with $\varepsilon = 5$, $\mu = -1$ and (a) $\xi = 0$, (b) $\xi = 0.18$, (c) $\xi = 0.4$ and (d) $\xi = \pi/2$. The vertical arrow in each panel denotes the position and sign of the δ -function. A noteworthy example is the soliton in panel (e), with a particularly large amplitude, obtained at $\xi = 0.282$, which is very close to ξ_{thr} . Panel (f) illustrates the stability of this soliton in direct simulations.

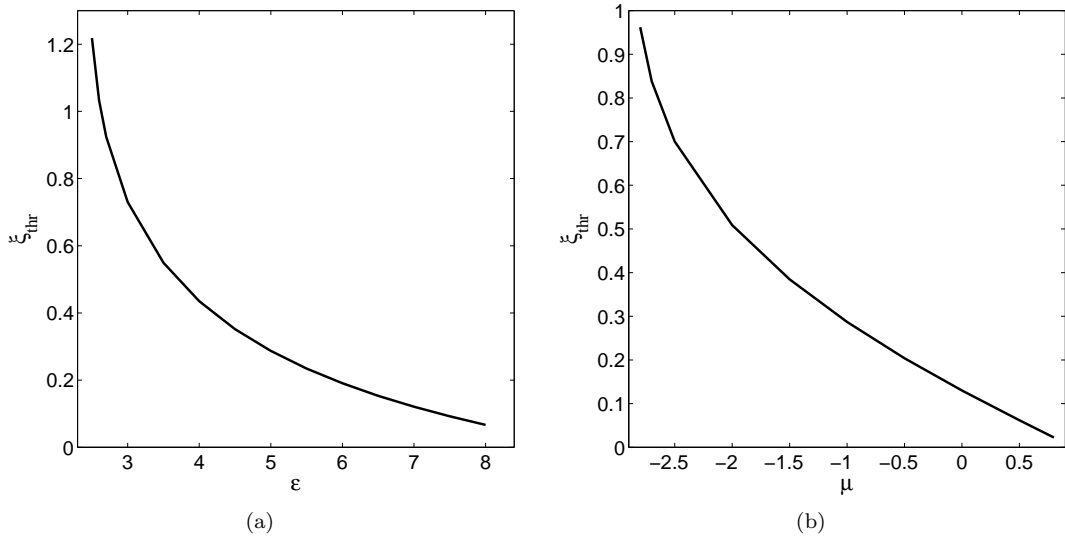


FIG. 11. (a) The existence threshold, ξ_{thr} , for the solitons in the first finite bandgap, as a function of ε , for $\mu = -1$. (b) The same, but as a function of μ for fixed $\varepsilon = 5$.

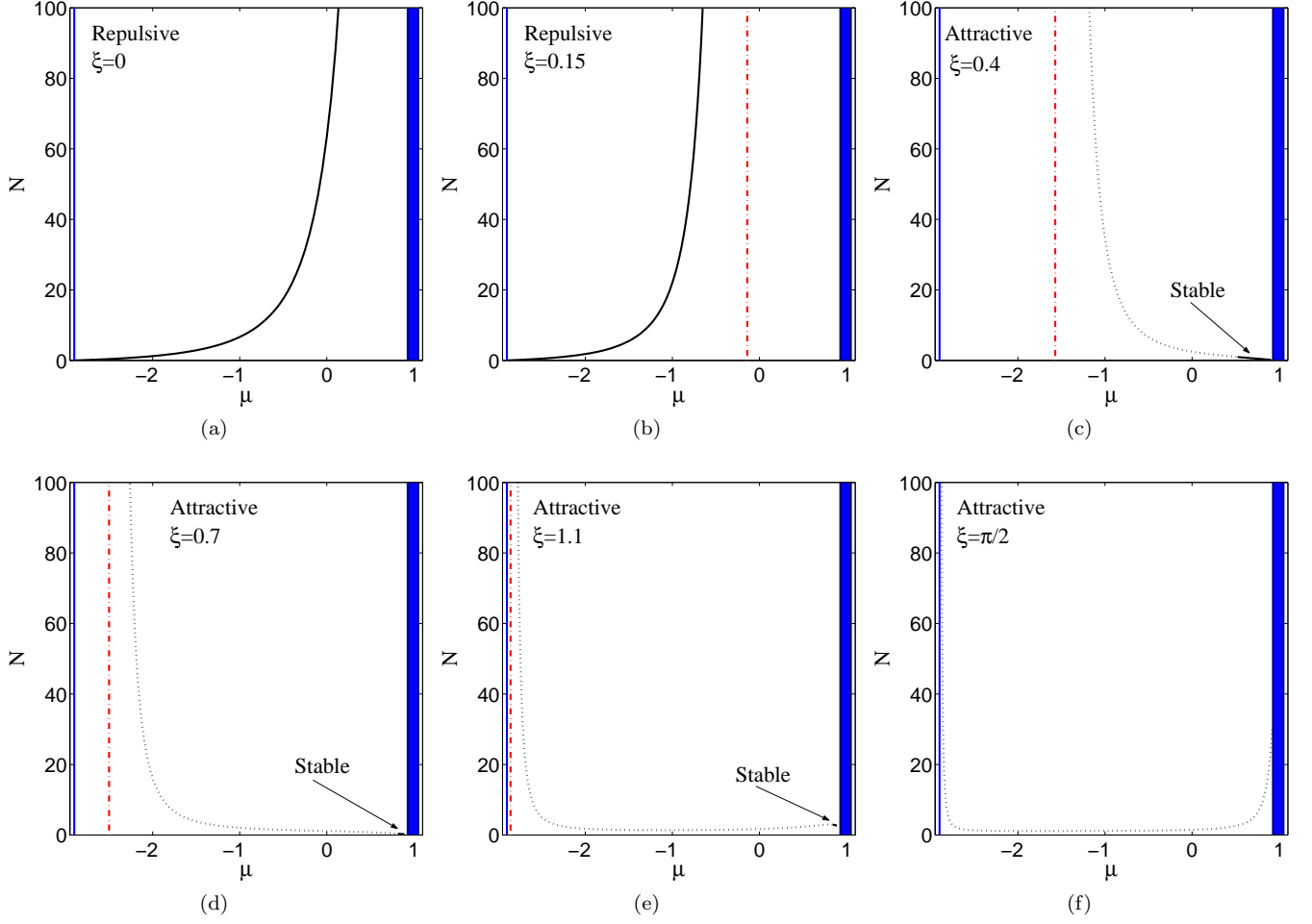


FIG. 12. (Color online) The norm of the gap solitons versus μ , in the first finite bandgap, for $\varepsilon = 5$, with the repulsive δ -function placed at $\xi = 0$ (a) or $\xi = 0.15$ (b), and the attractive δ -function placed at $\xi = 0.4$ (c), $\xi = 0.7$ (d), $\xi = 1.1$ (e), and $\xi = \pi/2$ (f). As above, the stable and unstable solitons correspond to continuous and dotted lines, respectively. A soliton subject to an oscillating instability can be found in the case (e), in an extremely narrow region (barely visible on the scale of this figure) between the stable and locally unstable sections. Blue vertical stripes between which the first bandgap is sandwiched. The dashed-dotted vertical lines represent thresholds at which the solitons' norm diverges: $\mu_{\text{thr}} = -0.141, -1.572, -2.5, -2.858$ for (b), (c), (d) and (e), respectively.

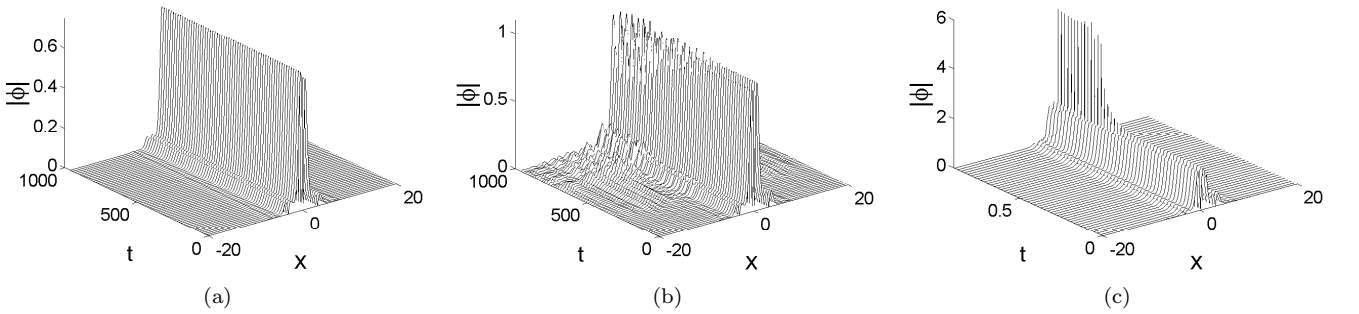


FIG. 13. The evolution of solitons supported by the single attractive δ -function, for the case shown in Fig. 9(b). Panel (a) displays an example of a stable soliton, obtained for $\xi = 0.4$. Unstable solitons, subject to the oscillatory instability or the strong localized instability, are exhibited for $\xi = 0.9$ (b) and $\xi = 1.3$ (c), respectively.

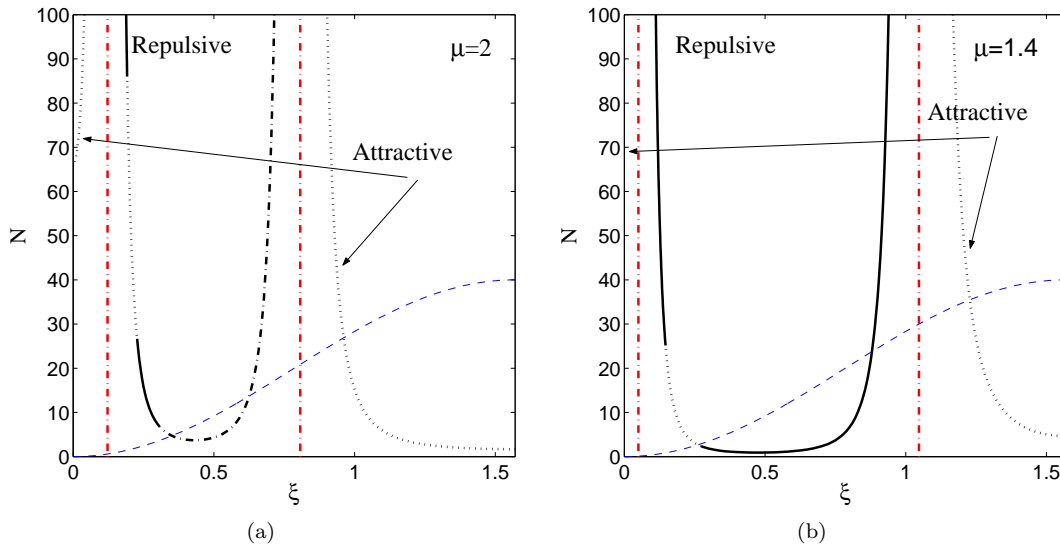


FIG. 14. (Color online) The same as in Fig. 9, but in the second finite bandgap, for $\mu = 2$ (a) and $\mu = 1.4$ (b). Note that, in very narrow regions of ξ , such as the left margin in (b), the norm of the (unstable) solitons, supported by the attractive instability, is especially large, therefore it cannot be displayed on the scale of this figure. The two thresholds (as explained in the text) are represented, as usual, by dashed-dotted vertical lines.

the middle of the second bandgap. In this bandgap, there are two thresholds in the region of $0 < \xi < \pi/2$. Similar to what was seen in the first bandgap, the soliton's amplitude diverges at the threshold, while the soliton's width remains finite.

With the attractive δ -function, GSs are always unstable in the second bandgap (featuring the localized instability), on the contrary to the situation in the first bandgap, where a small stability region was found for the case of attraction, see Figs. 9 and 12. On the other hand, in the case of the repulsive δ -function, the stability changes with the variation of parameters ξ , ε and μ . In particular, in the situation displayed in Fig. 14(a) both localized and oscillatory instabilities can be found, and *two* stability regions are present. If the repulsive δ -function is set at $\xi = 0.5$, and $\varepsilon = 5$, in which case the second bandgap is $1.05 < \mu < 3.724$, stable solitons are found only at μ close to the lower edge of the gap, see Fig. 15. For instance, at $\mu = 1.4$ the GSs are stable at almost all values of ξ , except for a narrow interval where the localized instability occurs, as seen in Fig. 14(b). Similar results were found at other values of ε .

Similar to the situation in the first bandgap, the GS families cover the entire second bandgap only for $\xi = 0$ and $\pi/2$. For different values of ξ , there are regions of μ in which no solitons are present, see Fig. 15.

V. NUMERICAL RESULTS FOR THE MODEL WITH THE TWO SYMMETRIC δ -FUNCTIONS

Equation (8) presents a natural extension of the model, which includes two δ -functions symmetrically positioned around the potential maxima or minima. We here consider the existence and stability conditions for solitons in this model, in the semi-infinite and the first finite gaps. In each case, two settings were explored, with either a potential maximum or minimum located exactly at the midpoint between the two δ -functions. The stability analysis was carried out using the method outlined in Sec. IV, with the nonlinearity coefficient $\delta(x - \xi)$ in Eq.(40) replaced by $\delta(x - \xi) + \delta(x + \xi)$.

A. Solitons in the semi-infinite gap

As in the models with the single δ -function, solitons in the semi-infinite gap exist only for the attractive nonlinearity. First, we examined the changes that the solitons undergo with the increase of distance ξ of each δ -function from the potential *minimum* located between them, which corresponds to $\varepsilon > 0$ in Eq. (8).

For small values of ξ , a region of stable symmetric solitons always exists. Increasing ξ , we reach a bifurcation point, after which the symmetric solutions lose their stability (against non-oscillatory perturbations) and a new *asymmetric* branch emerges, that may be partially stable. An example is shown in Fig. 16(a), for $\varepsilon = 5$ and $\mu = -4$. In this case,

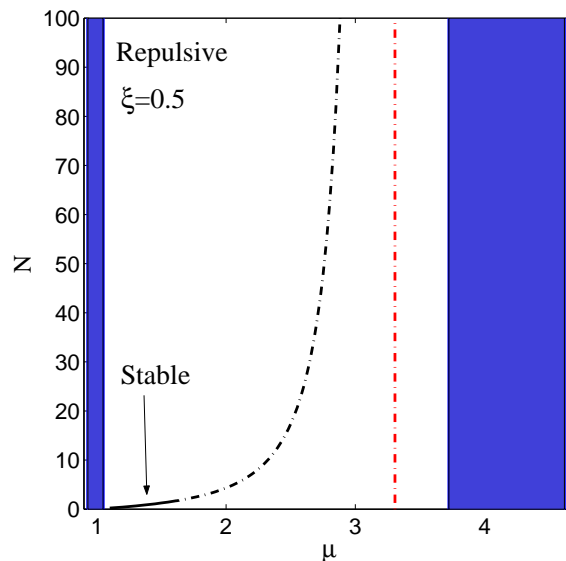


FIG. 15. (Color online) The norm versus μ , in the second finite bandgap for $\varepsilon = 5$, with the repulsive δ -function set at $\xi = 0.5$. The norm diverges at the threshold $\mu = 3.307$, marked by the vertical dashed-dotted curve.

there is a tiny region of stable asymmetric solitons, abutting on the bifurcation point, which is too small to be visible in the figure. Closer to the edge of the semi-infinite gap, the bifurcation occurs at higher values of ξ . For example, $\xi_{\text{bif}}(\varepsilon = 2, \mu = -1) = 0.777$, $\xi_{\text{bif}}(\varepsilon = 5, \mu = -3) = 0.935$, $\xi_{\text{bif}}(\varepsilon = 6, \mu = -4) = 0.683$, and $\xi_{\text{bif}}(\varepsilon = 8, \mu = -6) = 0.491$, and in all these cases, the asymmetric modes are completed unstable. On the other hand, the bifurcation occurs at smaller values of ξ for sets of (ε, μ) taken deeper inside gap, i.e., when ε is smaller and/or μ is more negative, the bifurcation giving rise to a conspicuous stability region for asymmetric states in such cases. Typical examples are presented in Fig. 18(a)-(b), for $(\varepsilon, \mu) = (2, -4)$ and $(5, -6)$. Going still deeper into the semi-infinite gap, the value of ξ at the bifurcation point keeps decreasing. The corresponding domain of stable asymmetric solutions may not necessarily emerge exactly at the bifurcation point, but slightly later. An example is displayed in Fig. 18(c) for $(\varepsilon, \mu) = (2, -6)$.

Bifurcation diagrams in the (μ, θ) plane, displayed in Fig. 18(d) for $\xi = 0.4$ and $\varepsilon = 2$ and 5 , demonstrate the SSB (spontaneous symmetry breaking) of supercritical type. For instance, at $\varepsilon = 2$, stable branches of the asymmetric modes emerge at the bifurcation point, where the symmetric branch loses its stability. On the other hand, for $\varepsilon = 5$ the asymmetric branches are not immediately stable after the bifurcation point, as the VK criterion is satisfied for them only when further decreasing μ .

At large values of ξ , the asymmetric soliton gradually transforms into a fundamental one, pinned to either of the two δ -functions. As concerns the symmetric modes, with the increase of the distance between the δ -functions (2ξ), they transform into two-soliton bound states which never regain the stability they had prior to the bifurcation. Specifically, near the OL minimum points, where the fundamental soliton is stable (see Fig. 16(a)), eigenvalues accounting for the instability of the bound state decrease as its two constituents are pulled farther apart with the increase of ξ (but still, never fall exactly to zero).

As in the two- δ -functions model without the lattice ($\varepsilon = 0$) [51], antisymmetric states exist too and are unstable at small values of ξ . As ξ increases, they develop into antisymmetric two-soliton bound states, for which unstable eigenmodes could not be found (featuring instead zero eigenvalues) exactly in the region where the stable fundamental soliton is supported by the single δ -function. Direct simulations have shown that, while such bound states are stable against symmetric disturbances, asymmetric perturbations break them into mutually incoherent fundamental solitons. Figure 17 presents several examples of the solitons of all the aforementioned types, in the case corresponding to Fig. 16(a).

Similar analysis was carried out for two attractive δ -functions placed on both sides of a local maximum of the periodic potential, which implies $\varepsilon < 0$ in Eq. (8). Figures 16(b) and 19 present a typical example of the results in the (ξ, N) plane, for $\varepsilon = -5$ and $\mu = -4$. In this case, both the symmetric and asymmetric solitons are unstable at small values of ξ . In other aspects, the results resemble those reported above for the case of two δ -functions placed symmetrically around a potential minimum.

It is relevant to compare these results with those reported in Ref. [51] for two attractive δ -functions in the absence of the periodic potential ($\varepsilon = 0$). In that case, exact analytical solutions are available for the pinned states of

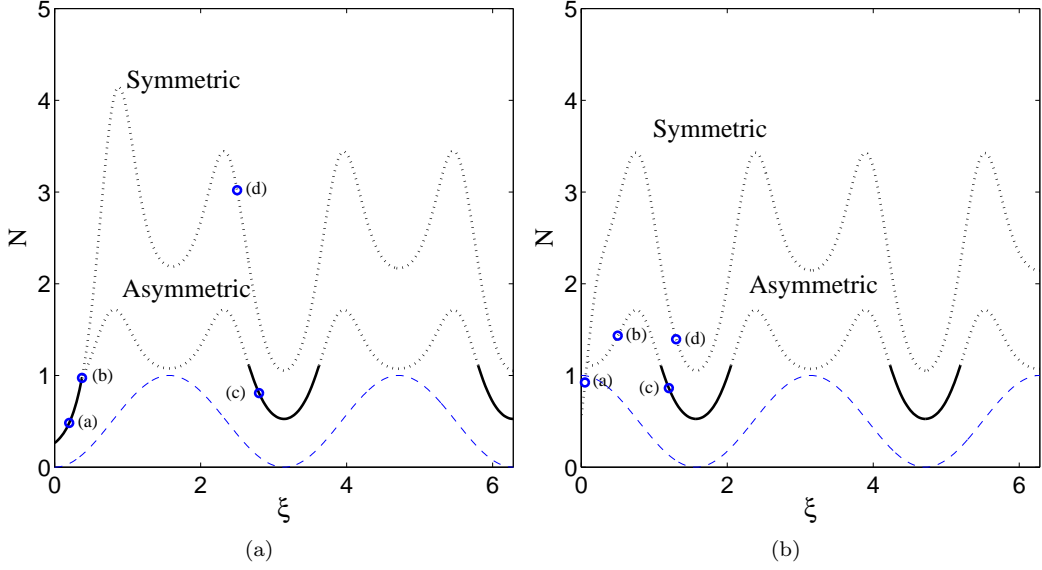


FIG. 16. Branches of symmetric and asymmetric soliton modes in the semi-infinite gap of the model with two δ -functions, for $\mu = -4$ and $\varepsilon = 5$ (a) or -5 (b), which correspond, respectively, to the local minimum or maximum of the periodic potential located between the δ -functions. As before, the continuous and dotted lines represent stable and unstable portions of the soliton families. Circles correspond to representative examples of solitons that are shown in panels (a)-(d) of Figs. 17 and 19 .

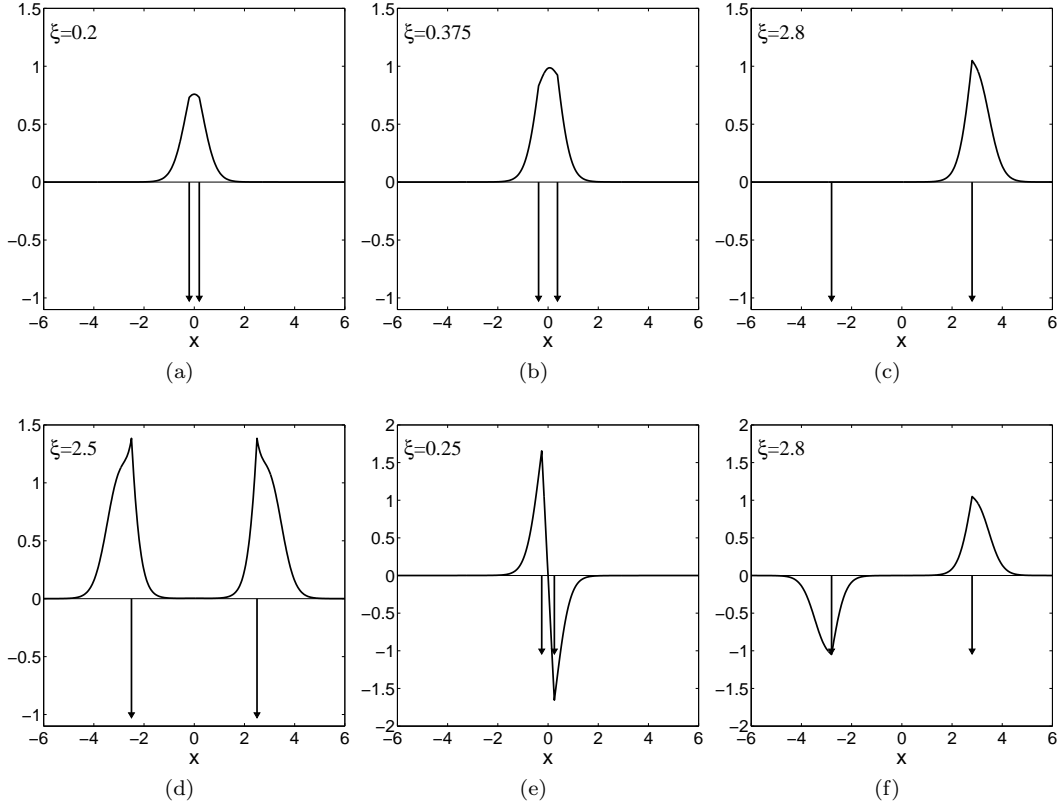


FIG. 17. Typical profiles of modes generated by two attractive δ -functions in the semi-infinite gap. Panels (a)-(d) correspond to the points marked by circles in Fig. 16(a). The arrows indicate the position of the δ -functions. Stable symmetric (a) and asymmetric (b)-(c) solitons are demonstrated, as well as an unstable symmetric bound state (d). In addition, panels (e) and (f) show, respectively, an unstable antisymmetric soliton, and an antisymmetric bound state which is unstable with respect to asymmetric perturbations.

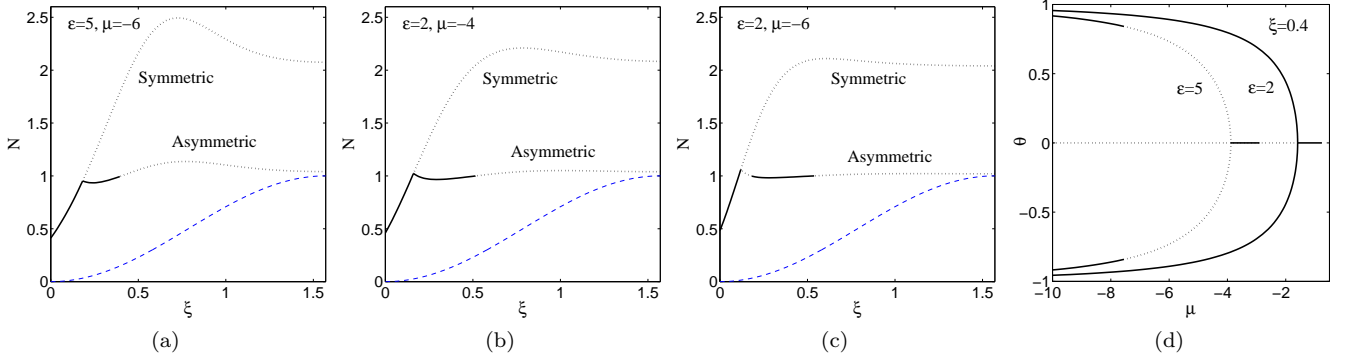


FIG. 18. (a)-(c) Branches of the symmetric and asymmetric states in the (ξ, N) plane near the bifurcation point, in the semi-infinite gap of the model with two δ -functions, for (a) $\varepsilon = 5$, $\mu = -6$, (b) $\varepsilon = 2$, $\mu = -4$, and (c) $\varepsilon = 2$, $\mu = -6$. (d) The bifurcation diagrams in the (μ, θ) plane, for $\xi = 0.4$ and $\varepsilon = 2$ and 5 .

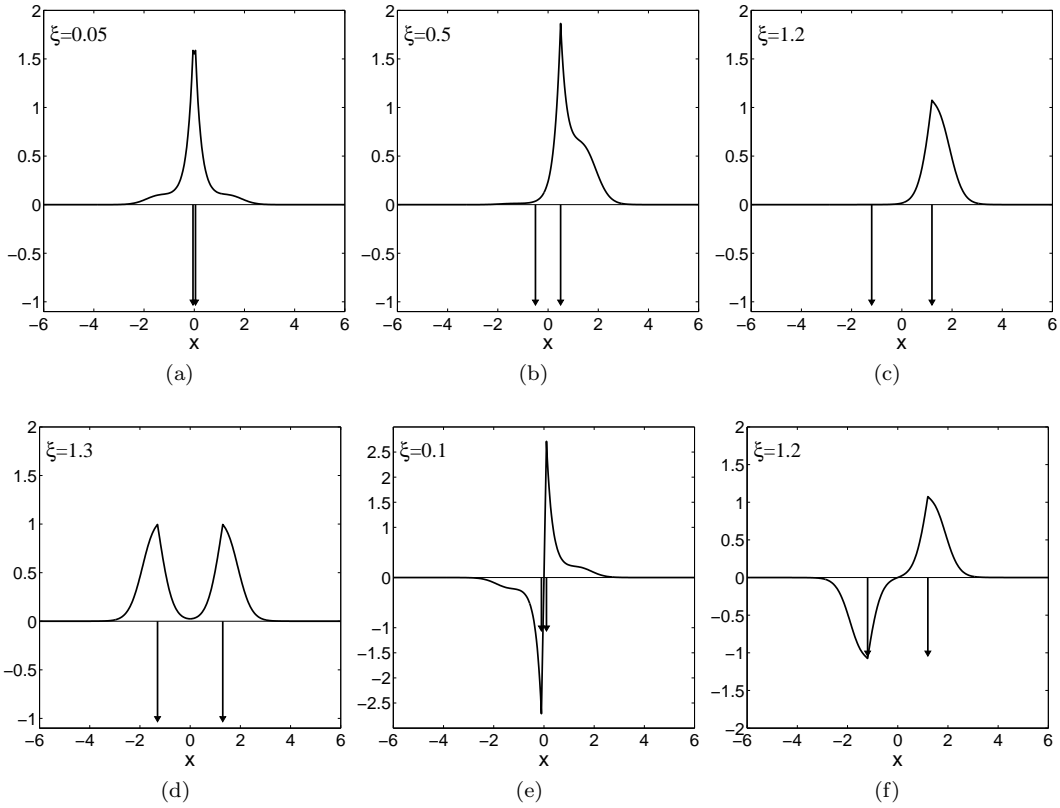


FIG. 19. Examples of solitons corresponding to the points marked by circles in Fig. 16(b). Panels (a) and (b) demonstrate unstable symmetric and asymmetric solitons. An example for a stable asymmetric soliton is displayed in (c). Panel (d) shows an unstable symmetric bound state. In addition, examples of an antisymmetric soliton, that features the strong local instability, and antisymmetric bound state, which is unstable against asymmetric perturbations, are shown in panels (e) and (f), respectively.

all the types—symmetric, asymmetric, and antisymmetric. The symmetric states are stable before the symmetry-breaking bifurcation, and unstable after it, terminating at final N . The bifurcation is of an “extreme subcritical” type, with branches of the asymmetric states going backwards and never turning forward, hence they are completely unstable. In fact, these results, obtained with the ideal δ -functions, are degenerate. The numerical analysis with regularized δ -functions lifts the degeneracy, demonstrating that the branches of the asymmetric modes eventually turn forward, stabilizing themselves. Simultaneously, the family of the symmetric modes (unstable past the bifurcation

point) extends to $N \rightarrow \infty$. Antisymmetric states are completely unstable in that model (they become stable if the regularized δ -functions are made broad enough). The comparison with the present findings suggests that the addition of the periodic potential also lifts the degeneracy of the system, even if the δ -functions are kept in the ideal form. In fact, this is similar to how the inclusion of the weak periodic potential lifts the degeneracy of the soliton family (4) supported by the single attractive δ -function and stabilizes the family, see Eqs. (36) and (37).

B. Solitons in the first finite bandgap

Similar to the case of the single δ -function, GSs in the first finite bandgap can be found for both the attractive and repulsive nonlinearities. We again start by considering the pair of δ -functions placed around a minimum of the potential. For the case of two attractive δ -functions, antisymmetric solitons exist in the region of $0 < \xi < \pi - \xi_{\text{thr}}$, where ξ_{thr} is the same threshold as in the model with the single δ -function. Unlike what was observed in the semi-infinite gap, in the first finite bandgap the asymmetric solitons bifurcate from the antisymmetric branch, see an example in Fig. 20(c) for $\varepsilon = 5$ and $\xi = 1$. In particular, this setting features a closed bifurcation loop, where both the direct and the reverse bifurcations are of the supercritical type. In the case presented in Fig. 20(c), there is a small region of stable antisymmetric solitons, obtained for high values of μ , near the upper edge of the gap. Decreasing μ , the soliton is destabilized by an oscillatory instability, both the antisymmetric and asymmetric branches being strongly unstable past the bifurcation point. A typical example, plotted in the (ξ, N) plane for $\varepsilon = 5$ and $\mu = -1$, is displayed in Figs. 20(a)-(b), where a small section of the antisymmetric branch is stable. The stability analysis, carried out for different values of ε and μ , indicates a somewhat larger stability region for larger ε , and for μ taken closer to the upper edge of the bandgap. The stability region gradually disappears at smaller values of ε , or close to the lower edge of the bandgap. A weak oscillatory instability also occurs in the present case. In particular, in the situation corresponding to Fig. 20, a very small section (too small to be visible in Fig. 20(a)) of the corresponding weakly unstable antisymmetric solitons exists, starting from the edge of the stable region and extending to slightly smaller values of ξ .

In this setting, an additional threshold, $\xi_{\text{thr}}^{(2)}$, was found (which is not related to that in the single- δ -function model, ξ_{thr} , see Fig. 11). The new threshold serves as the upper boundary for *always-stable* symmetric solitons generated by a pair of closely placed *repulsive* δ -functions, as shown in Fig. 20(b). Simultaneously, the same threshold is a lower border for a branch of unstable symmetric states that exists at $\xi_{\text{thr}}^{(2)} < \xi < \pi - \xi_{\text{thr}}$, in the case of the attractive nonlinearity. Typical examples of the soliton profiles of the symmetric, antisymmetric and asymmetric types are displayed in Fig. 21. Further, Fig. 22 shows $\xi_{\text{thr}}^{(2)}$ as a function of ε and μ (within the first finite bandgap). All the symmetric GSs are stable in the case of repulsion, and unstable under attraction.

Modes found at $\xi > \pi - \xi_{\text{thr}}$ may be considered as bound states of two fundamental GSs. For both signs of the nonlinearity, symmetric and antisymmetric bound states are found precisely where their fundamental counterparts exist. This can be seen in Fig. 20(a), comparing the location of the bound-state branches with those obtained in the model with the single δ -function, cf. Fig. 9(a). It is not surprising that both symmetric and antisymmetric bound states are strongly unstable close to the potential maximum, in the case of the attractive nonlinearity. For the repulsive nonlinearity, the symmetric bound states experience weak local instability in the regions near the minimum of the OL. On the other hand, their antisymmetric counterparts may appear to be stable in terms of the eigenvalues, and in direct simulations with respect to symmetric perturbations, but they split into their fundamental constituents when asymmetric disturbances are imposed (similar to the antisymmetric bound states in the semi-infinite gap.)

When the two δ -functions are placed around a maximum of the periodic potential, the picture is somewhat simpler. In this case, the secondary threshold, $\xi_{\text{thr}}^{(2)}$, does not exist, while, for the attractive nonlinearity, all types of the soliton families—symmetric, asymmetric and antisymmetric ones—exist in the region of $0 < \xi < \pi/2 - \xi_{\text{thr}}$ (not shown here). Also, on the contrary to the previous setting, the asymmetric solitons bifurcate from the symmetric branch (not from the antisymmetric one), all the solitons being unstable in the case of the attractive nonlinearity. Results for the bound states are qualitatively similar to those reported for the minimum-centered configuration, with the difference that, in the present case, the weak localized instability occurs for the antisymmetric solutions, while the symmetric bound states are the ones which are unstable only against asymmetric perturbations.

VI. CONCLUSIONS

In this work, we have introduced two settings that combine the attractive or repulsive nonlinearity, concentrated in one or two points, and the linear periodic potential. For the model with the single δ -function, we have found stable solutions in the semi-infinite and two lowest finite gaps. In particular, in the case of the attractive nonlinearity

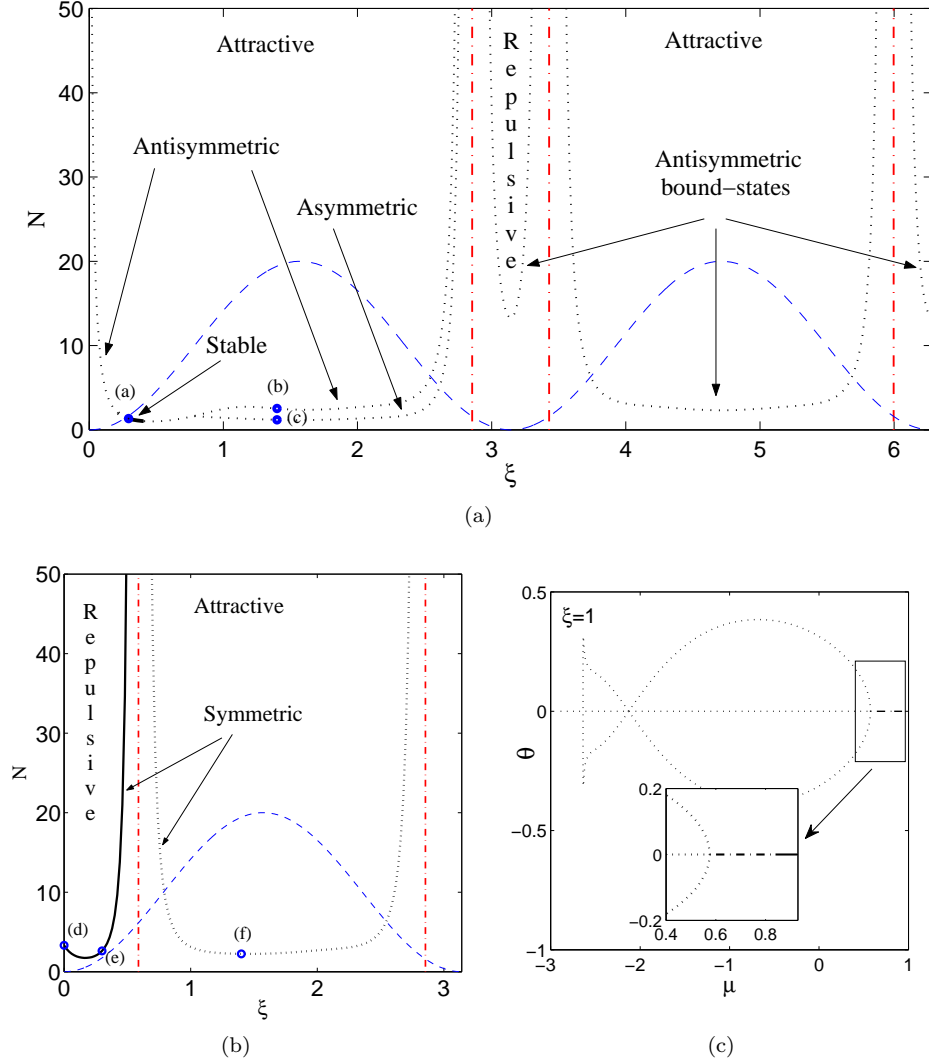


FIG. 20. (Color online) (a)-(b) The soliton's norm versus half the distance between the two δ -functions, ξ , in the first finite bandgap, for $\varepsilon = 5$ and $\mu = -1$. In panel (a), the asymmetric branch bifurcates from the antisymmetric one, in the case of the attractive nonlinearity. At larger values of ξ , the soliton branches correspond to unstable antisymmetric bound states of two solitons, for either repulsive or attractive nonlinearity. (b) Branches of symmetric states are shown for both the repulsive and attractive nonlinearities. Not shown in (b) are the unstable symmetric bound states, for larger ξ , as this part of the diagram is virtually identical to the one in panel (a), for the antisymmetric bound states. The dashed-dotted vertical lines represent the existence thresholds, $\pi \pm \xi_{\text{thr}} = 2.853, 3.43$ (periodic with period π) and $\xi_{\text{thr}}^{(2)} = 0.588$ [only in (b)]. Circles indicate solitons whose profiles are displayed in Fig. 21. (c) The bifurcation diagram for the antisymmetric and asymmetric modes, in the (μ, θ) plane, at $\varepsilon = 5$ and $\xi = 1$.

($\sigma = -1$), the degenerate family of exact soliton solutions exists in the absence of the periodic potential, being fully unstable. Even a weak potential lifts the degeneracy and stabilizes the entire family in the semi-infinite gap, provided that the δ -function is set in a finite region around a local minimum of the periodic potential. The stability of this soliton family agrees with the Vakhitov-Kolokolov criterion.

In the first finite bandgap, GSs (gap solitons) have been found for both attractive and repulsive nonlinearities, although they do not coexist: if the δ -function is placed in a finite area around a local minimum of the periodic potential, the GS exists only under the repulsion, and in the remainder of the period of the potential, GS can be supported solely by attractive nonlinearity. In the first bandgap, all the GSs are stable in the case of the repulsion, while the soliton pinned to the attractive δ -function is stable only in a small region, if any.

In the second bandgap, two soliton branches, centered around the attractive δ -function set at either the minimum or maximum of the periodic potential, were found. While none of them is stable, stability regions were produced for the soliton branch supported by the repulsive δ -function. It exists exactly for those values of shift ξ of the δ -function

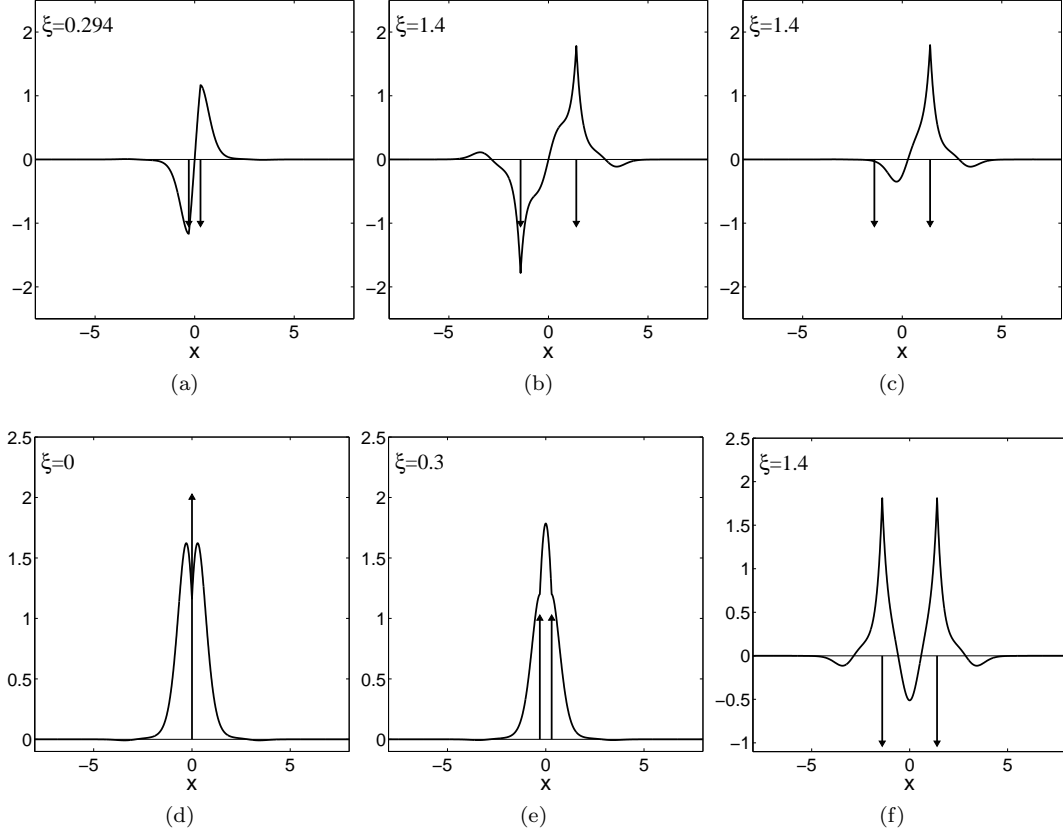


FIG. 21. Examples of solitons generated by two δ -functions in the first finite bandgap, which correspond to the marked points in Figs. 20(a), (b). As in Fig. 10, the arrows indicate the position and sign of the δ -functions. Stable and unstable antisymmetric solitons, as well as an unstable asymmetric one, are shown in (a), (b) and (c), respectively, in the case of two attractive δ -functions. Symmetric solitons, stable and unstable, are shown in panels (d),(e) and (f), for the repulsive and attractive nonlinearity, respectively.

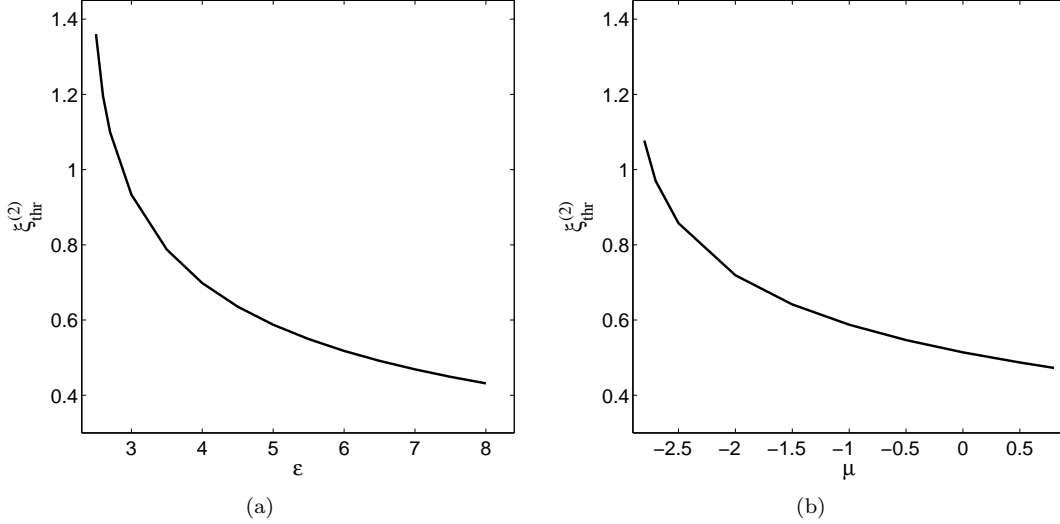


FIG. 22. (a) The secondary threshold, $\xi_{\text{thr}}^{(2)}$, for the pair of two closely set δ -functions in the first finite band gap, versus ε , for $\mu = -1$. (b) The same as a function of μ , for $\varepsilon = 5$.

relative to the underlying potential at which both aforementioned branches are absent in the case of the attraction.

In addition to the numerical results, analytical predictions, based on the perturbation theory for the Mathieu equation, were presented for the case when the δ -function is positioned exactly at the maximum or minimum of the periodic potential. This approximation was developed for the solitons in the semi-infinite and two lowest finite gaps, showing a good accuracy in comparison with the numerical findings, in all the cases.

In the model with two separated local nonlinearities, represented by the symmetric pair of the δ -functions, the numerical analysis was carried out for the semi-infinite and the first finite gaps. Families of symmetric, antisymmetric and asymmetric solitons were found, with respect to the symmetric set of the two δ -functions. In the semi-infinite gap, with the δ -functions set symmetrically around a minimum of the potential, the symmetric solitons are stable up to the symmetry-breaking bifurcation point, from which asymmetric branches emerge, that turn out to be partially stable. Antisymmetric modes were found too in the semi-infinite gap, being completely unstable. With the two δ -functions placed symmetrically around a point of the potential maximum, all the soliton families obtained at small separations between the δ -functions, as well as all the two-soliton bound states, are unstable.

In the first finite bandgap, asymmetric solitons bifurcate from the antisymmetric branch, if the potential minimum is set between the attractive δ -functions. This antisymmetric branch has a very short stability segment, while the asymmetric GSs are completely unstable. Under the repulsion, there is a stable branch of symmetric modes centered around the minimum of the potential. At a certain threshold value of the separation 2ξ between the δ -functions (which is different from the threshold found in the single- δ -function setting), the symmetric mode switches from the repulsive to attractive nonlinearity, simultaneously losing its stability. Finally, in the configuration with the local maximum of the periodic potential fixed at the midpoint, no stable solitons were found for sufficiently small separations 2ξ . For both configurations, with the midpoint coinciding with either the maximum or minimum of the underlying potential, all the families of two-soliton bound states are unstable against various perturbation modes.

This work may be naturally extended in other directions. In particular, it may be interesting to consider the nonlinearity represented by a periodic array of δ -functions. A challenging issue is to analyze similar models in two dimensions.

-
- [1] Y. S. Kivshar and G. P. Agrawal, *Optical Solitons: From Fibers to Photonic Crystals* (Academic Press: San Diego, 2003).
- [2] F. Lederer, G. I. Stegeman, D. N. Christodoulides, G. Assanto, M. Segev, and Y. Silberberg, Phys. Rep. **463**, 1 (2008); Y. V. Kartashov, V. A. Vysloukh, and L. Torner, Progress in Optics **52**, 63 (2009).
- [3] N. K. Efremidis, S. Sears, D. N. Christodoulides, J. W. Fleischer, and M. Segev, Phys. Rev. E **66**, 046602 (2002); J. W. Fleischer, M. Segev, N. K. Efremidis, and D. N. Christodoulides, Nature **422**, 147 (2003).
- [4] O. Morsch and M. Oberthaler, Rev. Mod. Phys. **78**, 179 (2006).
- [5] M. Lewenstein, A. Sanpera, V. Ahufinger, B. Damski, A. Sen, and U. Sen, Adv. Phys. **56**, 243 (2007).
- [6] S. Ghanbari, T. D. Kieu, A. Sidorov, and P. Hannaford, J. Phys. B: At. Mol. Opt. Phys. **39**, 847 (2006).
- [7] L. Bergé, Phys. Rep. **303**, 259 (1998).
- [8] F. K. Abdullaev and M. Salerno, Phys. Rev. A **72**, 033617 (2005).
- [9] B. B. Baizakov, B. A. Malomed, and M. Salerno, Europhys. Lett. **63**, 642 (2003).
- [10] N. K. Efremidis, J. Hudock, D. N. Christodoulides, J. W. Fleischer, O. Cohen and M. Segev, Phys. Rev. Lett. **91**, 213906 (2003).
- [11] J. Yang and Z. H. Musslimani, Opt. Lett. **28**, 2094 (2003); Z. H. Musslimani and J. Yang, J. Opt. Soc. Am. B **21**, 973 (2004).
- [12] B. B. Baizakov, B. A. Malomed and M. Salerno, Phys. Rev. A **70**, 053613 (2004).
- [13] D. Mihalache, D. Mazilu, F. Lederer, Y. V. Kartashov, L.-C. Crasovan and L. Torner, Phys. Rev. E **70**, 055603(R) (2004).
- [14] Y. V. Kartashov, V. A. Vysloukh, and L. Torner, Phys. Rev. Lett. **93**, 093904 (2004); **94**, 043902 (2005); Y. V. Kartashov, R. Carretero-González, B. A. Malomed, V. A. Vysloukh, and L. Torner, Opt. Express **13**, 10703 (2005).
- [15] B. B. Baizakov, B. A. Malomed, and M. Salerno, Phys. Rev. E **74**, 066615 (2006).
- [16] D. Mihalache, D. Mazilu, F. Lederer, B. A. Malomed, Y. V. Kartashov, L.-C. Crasovan, and L. Torner, Phys. Rev. Lett. **95**, 023902 (2005).
- [17] F. Kh. Abdullaev, B. B. Baizakov, S. A. Darmanyany, V. V. Konotop, and M. Salerno, Phys. Rev. A **64**, 043606 (2001); I. Carusotto, D. Embriaco, and G. C. La Rocca, *ibid.* **65**, 053611 (2002); P. J. Y. Louis, E. A. Ostrovskaya, C. M. Savage and Y. S. Kivshar Phys. Rev. A **67**, 013602 (2003).
- [18] D. E. Pelinovsky, A. A. Sukhorukov, and Y. S. Kivshar, Phys. Rev. E **70**, 036618 (2004).
- [19] N. K. Efremidis and D. N. Christodoulides, Phys. Rev. A **67**, 063608 (2003).
- [20] T. Mayteevarunyoo and B. A. Malomed, Phys. Rev. A **74**, 033616 (2006); *ibid.* **80**, 013827 (2009).
- [21] J. Cuevas, B.A. Malomed, P. G. Kevrekidis, and D. J. Frantzeskakis, Phys. Rev. A **79**, 053608 (2009).
- [22] M. Skorobogatiy and J. Yang, *Fundamentals of Photonic Crystal Guiding* (Cambridge University Press, 2009).
- [23] B. B. Baizakov, V. V. Konotop, and M. Salerno, J. Phys. B **35**, 5105 (2002); P. J. Y. Louis, E. A. Ostrovskaya, C. M. Savage, and Y. S. Kivshar, Phys. Rev. A **67**, 013602 (2003).
- [24] E. A. Ostrovskaya and Y. S. Kivshar, Opt. Exp. **12**, 19 (2004); Phys. Rev. Lett. **93**, 160405 (2004).
- [25] H. Sakaguchi and B.A. Malomed, J. Phys. B **37**, 2225 (2004).
- [26] A. Gubeskys, B.A. Malomed, and I. M. Merhasin, Phys. Rev. A **73**, 023607 (2006).
- [27] Z. Shi and J. Yang, Phys. Rev. E **75**, 056602 (2007).
- [28] J. Wang and J. Yang, Phys. Rev. A **77**, 033834 (2008).
- [29] E. A. Ostrovskaya, T. J. Alexander, and Y. S. Kivshar, Phys. Rev. **74**, 023605 (2006).
- [30] A. Gubeskys and B. A. Malomed, Phys. Rev. A **76**, 043623 (2007).
- [31] T. Mayteevarunyoo, B. A. Malomed, B. B. Baizakov, and M. Salerno, Physica D, **238**, 1439 (2008); J. Wang and J. Yang, Phys. Rev. A **77**, 033834 (2008).
- [32] B. Eiermann, Th. Anker, M. Albiez, M. Taglieber, P. Treutlein, K.-P. Marzlin, and M. K. Oberthaler, Phys. Rev. Lett. **92**, 230401 (2004).
- [33] Th. Anker, M. Albiez, R. Gati, S. Hunsmann, B. Eiermann, A. Trombettoni, and M. K. Oberthaler, Phys. Rev. Lett. **94**, 020403 (2005).
- [34] T. J. Alexander, E. A. Ostrovskaya, and Y. S. Kivshar, Phys. Rev. Lett. **96**, 040401 (2006).
- [35] B. A. Malomed, *Soliton Management in Nonlinear Systems* (Springer: New York, 2006).
- [36] W. A. Harrison, *Pseudopotentials in the Theory of Metals* (Benjamin: New York, 1966).
- [37] Y. V. Kartashov, B. A. Malomed, and L. Torner, *Solitons in nonlinear lattices*, Rev. Mod. Phys., in press.
- [38] B. I. Mantsyzov and R. N. Kuz'min, Sov. Phys. JETP **64**, 37 (1986); B. I. Mantsyzov, Phys. Rev. A **51**, 4939 (1995); A. Kozhokin and G. Kurizki, Phys. Rev. Lett. **74**, 5020 (1995); T. Opatrny, B. A. Malomed, and G. Kurizki, Phys. Rev. E **60**, 6137 (1999); A. Y. Sivachenko, M. E. Raikh, and Z. V. Vardeny, Phys. Rev. A **64**, 013809 (2001); J. Cheng and J. Y. Zhou, Phys. Rev. E **66**, 036606 (2002).
- [39] G. Kurizki, A. E. Kozhokin, T. Opatrny, and B. A. Malomed, in Progress in Optics 42, 93 (E. Wolf, editor: North Holland, Amsterdam, 2001).
- [40] K. Busch, G. von Freymann, S. Linden, S. F. Mingaleev, L. Tkeshelashvili, and M. Wegener, Phys. Rep. **444**, 101 (2007).
- [41] S. Inouye, M. R. Andrews, J. Stenger, H. J. Miesner, D. M. Stamper-Kurn, and W. Ketterle, Nature (London) **392**, 151 (1998); Ph. Courteille, R. S. Freeland, D. J. Heinzen, F. A. van Abeelen, and B. J. Verhaar, Phys. Rev. Lett. **81**, 69 (1998); J. L. Roberts, N. R. Claussen, J. P. Burke, C. H. Greene, E. A. Cornell, and C. E. Wieman, *ibid.* **81**, 5109 (1998).
- [42] P. O. Fedichev, Yu. Kagan, G. V. Shlyapnikov, and J. T. M. Walraven, Phys. Rev. Lett. **77**, 2913 (1996).
- [43] M. Theis, G. Thalhammer, K. Winkler, M. Hellwig, G. Ruff, R. Grimm, and J. H. Denschlag, Phys. Rev. Lett. **93**, 123001

- (2004).
- [44] M. Marinescu and L. You, Phys. Rev. Lett. **81**, 4596 (1998).
 - [45] K. E. Strecker, G. B. Partridge, A. G. Truscott, and R. G. Hulet, Nature **417**, 150 (2002); L. Khaykovich, F. Schreck, G. Ferrari, T. Bourdel, J. Cubizolles, L. D. Carr, Y. Castin, and C. Salomon, Science **296**, 1290 (2002).
 - [46] H. Sakaguchi and B. A. Malomed, Phys. Rev. E **72**, 046610 (2005); J. Garnier and F. K. Abdullaev, Phys. Rev. A **74**, 013604 (2006); D. L. Machacek, E. A. Foreman, Q. E. Hoq, P. G. Kevrekidis, A. Saxena, D. J. Frantzeskakis, and A. R. Bishop, Phys. Rev. E **74**, 036602 (2006); M. A. Porter, P. G. Kevrekidis, B. A. Malomed, and D. J. Frantzeskakis, Physica D **229**, 104 (2007); J. Belmonte-Beitia, V. M. Pérez-García, V. Vekslerchik, and P. J. Torres, Phys. Rev. Lett. **98**, 064102 (2007); F. Abdullaev, A. Abdumalikov, and R. Galimzyanov, Phys. Lett. A **367**, 149 (2007); G. Dong and B. Hu, Phys. Rev. A **75**, 013625 (2007); D. A. Zezyulin, G. L. Alfimov, V. V. Konotop, and V. M. Pérez-García, *ibid.* **76**, 013621 (2007); Z. Rapti, P. G. Kevrekidis, V. V. Konotop, and C. K. R. T. Jones, J. Phys. A: Math. Theor. **40**, 14151 (2007); H. A. Cruz, V. A. Brazhnyi, and V. V. Konotop, J. Phys. B: At. Mol. Opt. Phys. **41**, 035304 (2008); L. C. Qian, M. L. Wall, S. L. Zhang, Z. W. Zhou, and H. Pu, Phys. Rev. A **77**, 013611 (2008); F. K. Abdullaev, A. Gammal, M. Salerno, and L. Tomio, *ibid.* **77**, 023615 (2008); A. S. Rodrigues, P. G. Kevrekidis, M. A. Porter, D. J. Frantzeskakis, P. Schmelcher, and A. R. Bishop, *ibid.* **78**, 013611 (2008); Y. V. Kartashov, B. A. Malomed, V. A. Vysloukh, and L. Torner, Opt. Lett. **34**, 3625 (2009).
 - [47] R. Y. Hao, R. C. Yang, L. Li, and G. S. Zhou, Opt. Commun. **281**, 1256 (2008).
 - [48] H. Sakaguchi and B. A. Malomed, Phys. Rev. E **73**, 026601 (2006); G. Fibich, Y. Sivan, and M. I. Weinstein, Physica D **217**, 31 (2006); G. Dong, B. Hu, and W. Lu, Phys. Rev. A **74**, 063601 (2006); R. Y. Hao and G. S. Zhou, Chin. Opt. Lett. **6**, 211 (2008); Y. V. Kartashov, B. A. Malomed, V. A. Vysloukh, and L. Torner, Opt. Lett. **34**, 770 (2009); N. V. Hung, P. Ziñ, M. Trippenbach, and B. A. Malomed, Phys. Rev. E **82**, 046602 (2010).
 - [49] B.A. Malomed and M. Ya. Azbel, Phys. Rev. B **47**, 10402 (1993).
 - [50] A. A. Sukhorukov, Y. S. Kivshar, and O. Bang, Phys. Rev. E **60**, R41 (1999).
 - [51] T. Maytevarunyoo, B. A. Malomed, and G. Dong, Phys. Rev. A **78**, 053601 (2008).
 - [52] L. C. Qian, M. L. Wall, S. Zhang, Z. Zhou, and H. Pu, Phys. Rev. A **77**, 013611 (2008).
 - [53] M. Vakhitov and A. Kolokolov, Radiophys. Quantum. Electron. **16**, 783 (1973).
 - [54] L. D. Landau and E. M. Lifshitz, Mechanics (Nauka Publishers: Moscow, 1973).
 - [55] H. Sakaguchi and B. A. Malomed, Phys. Rev. A **81**, 013624 (2010).